

Contents lists available at ScienceDirect

# Journal of Constructional Steel Research



# Numerical modeling of stress-strain relationships for advanced high strength steels



Yu Xia <sup>a</sup>, Chu Ding <sup>b</sup>, Zhanjie Li <sup>c</sup>, Benjamin W. Schafer <sup>b</sup>, Hannah B. Blum <sup>a,\*</sup>

- <sup>a</sup> Department of Civil and Environmental Engineering, University of Wisconsin-Madison, USA
- <sup>b</sup> Department of Civil and Systems Engineering, Johns Hopkins University, USA
- <sup>c</sup> Department of Engineering, SUNY Polytechnic Institute, USA

#### ARTICLE INFO

#### Article history: Received 30 December 2020 Received in revised form 27 March 2021 Accepted 1 April 2021 Available online 20 April 2021

Keywords:
Cold-formed steel
Stress-strain modeling
Tensile coupon test
Advanced high-strength steel
Ramberg-Osgood model

#### ABSTRACT

As a result of altered chemical composition, multiphase microstructures, and other micromechanical change, advanced high strength steel (AHSS) has three to five times the strength of conventional mild steels. Developed for automotive applications, AHSS has high potential for application in cold-formed steel construction. However, the material properties must be properly understood and quantified for application to structural design with economic efficiency. A series of tensile coupon tests were carried out to determine typical AHSS material properties. Existing stress-strain models, designed for steels with gradual strain hardening, were studied and recalibrated to the AHSS test data. No existing method provided an accurate fit for all cases. An updated two-stage plus linear stress-strain model, based on the Ramberg-Osgood expression, was developed. The predictive equations for the parameters required by the new model were provided based on the statistical analysis of AHSS test data. In addition, from the discussion of the new model, a novel proof stress was recommended to represent the yield strength of AHSS. Energy was used to compare the AHSS experimental stress-strain curves with conventional steel stress-strain models to examine the rationality of the proposed proof stress as the yield strength in design.

© 2021 Elsevier Ltd. All rights reserved.

## 1. Introduction

Thin-walled cold-formed steel (CFS) members formed from coils of mild steel have been widely used in the structural and construction industries in the United States and globally since the 1940s. In general, CFS members have unique advantages, including nestable sections for compact packaging and shipping, lightweight and consequently high strength-to-weight ratios, and high recyclability [1]. Owing to material science advances at the microstructural level over the past two decades, advanced high strength steel (AHSS) has been developed. AHSS are steels with unique microstructures utilizing complex deformation and phase transformation processes to achieve unprecedented combinations of strength and ductility. The design and manufacture of AHSS require circumspect selection of chemical compositions and precisely controlled heating and cooling processes. Subsequently, AHSS exhibit a multiphase microstructure containing one or more phases different from ferrite, pearlite, or cementite. Rather, these phases, for example, include martensite, bainite, austenite, and/or retained austenite that are sufficient in quantities to produce unique mechanical properties. AHSS includes new grades of sheet steel with yield strength up to 1250 MPa, ultimate strength up to 1900 MPa, and tensile elongation upwards of 20% to 30%. In addition, different from conventional steels, the terminology AHSS is classified by its metallurgical designation, rather than the steel grades. As a result, AHSS can have a wider range of grades (e.g., with ultimate strength as low as 440 MPa and yield strength as low as 210 MPa) than the conventional high strength steels, which require a yield strength higher than 460 MPa [2]. AHSS have been maturely developed and applied in the automobile industry for its excellence in stiffness, crash performance and formability [3]. The civil construction industry requires different design constraints than the automobile industry, therefore research needs to be carried out on the application of AHSS members as load-bearing components in structural framing for civil construction. For any attempt to characterize the structural performance of AHSS CFS members, a database of AHSS material properties is a prerequisite, which is explicitly discussed in this paper.

AHSS includes various families of steel, including Dual Phase (DP), Complex Phase (CP), Ferritic-Bainitic (FB), Martensitic (MS), Transformation-Induced Plasticity (TRIP) and more. Different families of AHSS are made with specifically selected chemical composition and manufacturing processes, which result in unique material properties. Among various AHSS families, DP and MS currently have lowest manufacturing cost and therefore are advised to be firstly studied for structural engineering applications as they have the lowest cost barrier to entry. DP steels comprise a ferritic matrix which encompass a hard martensite second phase and generally a higher percentage

<sup>\*</sup> Corresponding author. E-mail address: hannah.blum@wisc.edu (H.B. Blum).

composition of the hard martensite second phase demonstrates higher steel strength. DP steels are produced by a controlled cooling process from the initial two-phase ferrite plus austenite phase to transform some austenite to ferrite before transforming the remaining austenite to martensite. DP steels typically have a high degree of ductility and may have a lower cost and higher availability than other AHSS. MS steels comprise a martensitic matrix containing ferrite and bainite and generally have the highest strengths. MS steels are produced from the austenite phase to transform most of the austenite to martensite. The chemical composition of MS steels also includes carbon, manganese, silicon and/or other elements to increase steel hardenability and strengths. MS steels typically have somewhat lowered ultimate elongations at fracture [2].

In this paper, a series of tensile coupon tests on specimens made from two different families of AHSS (DP and MS) is presented. The tests were conducted per ASTM E8 [4]; and additional procedures and techniques recommended by Huang and Young [5] were also adopted. A numerical model of the stress-strain relationship for AHSS is proposed. Existing models on steels with gradual yielding, including conventional CFS and stainless steel, are discussed. Numerical studies show that existing models discussed in this paper do not accurately fit AHSS  $\sigma$ - $\varepsilon$  curves from the tests conducted herein. Therefore, this paper proposes an updated two-stage plus linear stress-strain model for AHSS. Excellent fit between the proposed model and the AHSS test  $\sigma$ - $\varepsilon$  curves are achieved. For scenarios when the full  $\sigma$ - $\varepsilon$  curve is unavailable, predictive equations for the parameters in the proposed model are also proposed based on statistical analysis of the AHSS test data. From the discussion on the proposed model, the possibility of adopting a new proof stress level to represent yield strength is also raised. A discussion of the proposed proof stress is carried out comparing the energy dissipation between the AHSS test curves and conventional stressstrain models.

## 2. Existing stress-strain models

Accurate modeling of the constitutive relationship for metallic materials is essential in advanced structural design and numerical analysis. Different from conventional mild steels with a clear yield point and yield plateau, the  $\sigma$ - $\varepsilon$  relationship for sheet steel are generally more rounded with an increased yield strength, an increased ultimate strength and a decreased proportional limit. To depict the non-linear  $\sigma$ - $\varepsilon$  relationship for CFS, various models have been proposed. Among these models, the Ramberg-Osgood (R-O) model [6] is widely recognized and extensively used, not only for CFS but also other metals with similar stress-strain behaviors including stainless steel and aluminum. The universal form of the R-O model is shown in Eq. (1):

$$\varepsilon = \frac{\sigma}{E} + p \left(\frac{\sigma}{\sigma_p}\right)^n \quad \text{for } 0 \le \sigma \le \sigma_u$$
 (1)

where  $\sigma$  denotes stress and  $\varepsilon$  denotes strain, E is elastic modulus,  $\sigma_p$  is the proof stress which corresponds to a plastic strain of p, and n is the exponential coefficient which determines the degree of curvature for the stress-strain model.

For p=0.002, Fig. 1 shows the effect of hardening parameter n on the  $\sigma$ - $\varepsilon$  curve. When n<1, the  $\sigma$ - $\varepsilon$  curve is concave; when n=1, the  $\sigma$ - $\varepsilon$  curve is a straight line between the origin and the ultimate point, which is the end of the model; and when n>1, the  $\sigma$ - $\varepsilon$  curve is convex. For the convex case (i.e. n>1), as n increases, the degree of curve convexity becomes less sensitive to the increment of n; and when n approaches positive infinity, the curve is comprised by two straight lines. Thus, n=1 is elastic and  $n\to +\infty$  is elastic-perfectly-plastic. The  $\sigma$ - $\varepsilon$  curve will pass through the origin and the 0.2% proof stress  $\sigma_{0.2}$ , regardless the value of n. The R-O model is only able to depict the constitutive relationship when it is monotonically increasing. The R-O model is unable to depict the strain softening process after the ultimate point. These two constraints are applicable to all updated models originating

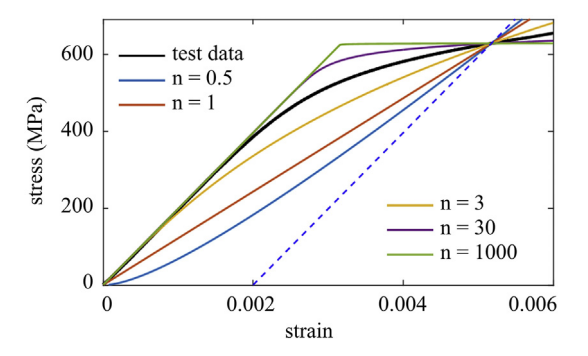


Fig. 1. Different scenarios of Ramberg-Osgood expression using different n.

from the R-O model. The most commonly used evolution of Eq. (1) was proposed by Hill [7], where p = 0.002 was used as shown in Eq. (2).

$$\varepsilon = \frac{\sigma}{E} + 0.002 \left(\frac{\sigma}{\sigma_{0.2}}\right)^n \quad \text{for } 0 \le \sigma \le \sigma_u$$
 (2)

Previous studies [8–10] have shown that Eq. (2) is able to provide accurate approximations of experimental  $\sigma$ - $\varepsilon$  curves at relatively lower stress levels (e.g. up to 0.2% proof stress), and is inaccurate at higher stress regions for CFS sheets. Therefore, the original one stage R-O model is not able to accurately depict the entire  $\sigma$ - $\varepsilon$  behavior of steel up to ultimate. As such, researchers have made updates to the original R-O model. Among all these updates, the central idea is to divide the curve into several stages and model them separately.

A two-stage model R-O was first proposed by Mirambell and Real [8]. They conducted a series of tensile coupon tests of cold-formed stainless steel Type 304/304L and proposed Eq. (2) for stress up to  $\sigma_{0.2}$  and a new Eq. (3) for stress between  $\sigma_{0.2}$  and ultimate strength  $\sigma_u$ :

$$\varepsilon = \frac{\sigma - \sigma_{0.2}}{E_{0.2}} + \varepsilon_{pu} \left( \frac{\sigma - \sigma_{0.2}}{\sigma_u - \sigma_{0.2}} \right)^m + \varepsilon_{0.2} \quad \text{for } \sigma_{0.2} \le \sigma \le \sigma_u$$
 (3)

where  $E_{0.2}$  is the tangent modulus at  $\sigma_{0.2}$ ,  $\varepsilon_{pu}$  is the total plastic strain of ultimate point,  $\varepsilon_{0.2}$  is the total strain corresponds to  $\sigma_{0.2}$ , and m is the exponential coefficient determining the degree of curvature of the  $\sigma$ - $\varepsilon$  curve between the 0.2% offset and the ultimate.

Rasmussen [9] independently proposed an approximate expression of Eq. (3) for austenitic, duplex, and ferritic stainless steel alloy as shown in Eq. (4) by neglecting the difference between the ultimate strain  $\varepsilon_u$  and the plastic strain of the ultimate point  $\varepsilon_{pu}$  ( $\varepsilon_{pu} \approx \varepsilon_u$ ) because stainless steels are generally ductile.

$$\varepsilon = \frac{\sigma - \sigma_{0.2}}{E_{0.2}} + \varepsilon_u \left(\frac{\sigma - \sigma_{0.2}}{\sigma_u - \sigma_{0.2}}\right)^m + \varepsilon_{0.2} \quad \text{for } \sigma_{0.2} \le \sigma \le \sigma_u$$
 (4)

Rasmussen also proposed an expression of  $E_{0.2}$  as shown in Eq. (5). To calculate the slope of the curve at  $\sigma_{0.2}$ ,  $E_{0.2}$  and m in Eq. (4) are unknown before they are calculated, therefore instead of Eq. (4), Eq. (2) is used as the strain expression in Eq. (5).

$$\frac{1}{E_{0.2}} = \frac{\partial \varepsilon(\sigma)}{\partial \sigma} \left| \sigma = \sigma_{0.2} = \frac{1 + 0.002n \frac{\sigma}{\sigma_{0.2}^n} E}{E} \right|_{\sigma = \sigma_{0.2}} = \frac{1 + 0.002n \frac{E}{\sigma_{0.2}}}{E} \Rightarrow E_{0.2}$$

$$= \frac{E}{1 + 0.002n \frac{E}{\sigma_{0.2}}} \tag{5}$$

Gardner and Nethercot [10] studied the material properties of Grade 1.4301 stainless steel and updated Eq. (3) so that the model passes through the ultimate point. For mathematical consistency, the second stage expression is updated as shown in Eq. (6).

$$\varepsilon = \frac{\sigma - \sigma_{0.2}}{E_{0.2}} + \left(\varepsilon_{u} - \varepsilon_{0.2} - \frac{\sigma_{u} - \sigma_{0.2}}{E_{0.2}}\right) \left(\frac{\sigma - \sigma_{0.2}}{\sigma_{u} - \sigma_{0.2}}\right)^{m} + \varepsilon_{0.2} \quad \text{for } \sigma_{0.2} \le \sigma \le \sigma_{u}$$
(6)

Additionally, Gardner further updated the second stage expression by forcing the expression to pass through  $\sigma_{0.2}$  and the 1% proof stress  $\sigma_{1.0}$  as shown in Eq. (7) to expand the applicability of the model to include compression stress-strain behavior, where  $\sigma_{n}$  is generally unavailable.

$$\varepsilon = \frac{\sigma - \sigma_{0.2}}{E_{0.2}} + \left(0.008 - \frac{\sigma_{1.0} - \sigma_{0.2}}{E_{0.2}}\right) \left(\frac{\sigma - \sigma_{0.2}}{\sigma_{1.0} - \sigma_{0.2}}\right)^{m} + \varepsilon_{0.2} \quad \text{for } \sigma_{0.2} \le \sigma \le \sigma_{u}$$
(7)

Inspired by the work of Gardner and Nethercot [10], Li and Young [11] proposed a two-stage stress-strain model (as shown in Eq. (8), where the subscript T indicates the material property at temperature T 'C) designed for cold-formed high strength steel at both ambient and elevated temperature, and a series of predictive equations for the parameters required by the model were provided. The proposed two-stage model was verified by the accurate fits with experimental stress-strain curves at both ambient and at elevated temperatures up to  $1000^{\circ}\text{C}$  of two series of cold-formed high strength steels with nominal yield strength of 700 MPa and 900 MPa at ambient.

$$\varepsilon = \begin{cases} \frac{\sigma}{E_T} + 0.002 \left(\frac{\sigma}{\sigma_{0.2T}}\right)^n & \text{for } 0 \le \sigma \le \sigma_{0.2T} \\ \frac{\sigma - \sigma_{0.2T}}{E_{0.2T}} + \left(\varepsilon_{uT} - \varepsilon_{0.2T} - \frac{\sigma_{uT} - \sigma_{0.2T}}{E_{0.2T}}\right) \left(\frac{\sigma - \sigma_{0.2T}}{\sigma_{uT} - \sigma_{0.2T}}\right)^m + \varepsilon_{0.2T} & \text{for } \sigma_{0.2T} < \sigma \le \sigma_{uT} \end{cases}$$

$$(8)$$

Besides two-stage models, multiple-stage models were also proposed to further improve curve fit accuracy. Hradil et al. [12] updated Mirambell's two-stage model [8] and proposed a generalized multiple-stage stress-strain model which was flexible to accommodate any amount of measured or recommended parameters. In their paper, a three-stage model was used as an example of the multiple stage model. Stress-strain data from the origin to the ultimate was split into three stages by  $\sigma_{0.2}$  and  $\sigma_{1.0}$ . The first stage expression is given in Eq. (2), the second stage expressions is given in Eq. (9), and the third stage expression is given in Eq. (10). The definitions of some new parameters, including  $\varepsilon_{0.2}^{\star}$ ,  $\varepsilon_{1.0}^{\star}$ ,  $n_2$ , and  $n_3$ , are introduced in the original source [12]. A set of explicit equations as the inversion of Eqs. (2), (9), and (10) were also provided.

$$\varepsilon = \frac{\sigma - \sigma_{0.2}}{E_{0.2}} + \varepsilon_{0.2} \star \left(\frac{\sigma - \sigma_{0.2}}{\sigma_{1.0} - \sigma_{0.2}}\right)^{n_2} + 0.002 + \frac{\sigma_{0.2}}{E} \quad \text{for } \sigma_{0.2} \le \sigma \le \sigma_{1.0}$$
(9)

$$\varepsilon = \frac{\sigma - \sigma_{1.0}}{E_{1.0}} + \varepsilon_{1.0}^* \left(\frac{\sigma - \sigma_{1.0}}{\sigma_u - \sigma_{1.0}}\right)^{n_3} + 0.01 + \frac{\sigma_{1.0}}{E} \quad \text{for } \sigma_{1.0} < \sigma \le \sigma_u$$

$$(10)$$

Quach [13] further updated the model for stainless steel from the works of Olsson [14] and Gardner [15], and came up with a new three-stage model. The first stage expression is given by Eq. (2). The second stage ranges from  $\sigma_{0.2}$  to 2.0% proof stress  $\sigma_{2.0}$  and the expression is given by Eq. (11).

$$\varepsilon = \frac{\sigma - \sigma_{0.2}}{E_{0.2}} + \left(0.008 + (\sigma_{1.0} - \sigma_{0.2}) \left(\frac{1}{E} - \frac{1}{E_{0.2}}\right)\right) \left(\frac{\sigma - \sigma_{0.2}}{\sigma_{1.0} - \sigma_{0.2}}\right)^{m} + \varepsilon_{0.2} \quad \text{for } \sigma_{0.2} \le \sigma \le \sigma_{2.0}$$
(11)

A similar expression of the second stage was also adopted in [15,16]. The third stage ranges from  $\sigma_{2.0}$  to  $\sigma_u$ . The third stage expression is based on a linear relationship between true stress  $\sigma^t$  and engineering strain  $\varepsilon$ , ( $\sigma^t = a + b\varepsilon$ ) and is given by Eq. (12):

$$\varepsilon = \frac{\sigma - a}{b - \sigma} \quad \text{for } \sigma_{2.0} < \sigma \le \sigma_u \tag{12}$$

where parameters a and b are calculated by Eqs. (13) and (14) using material properties including  $\varepsilon_{2.0}$  (the strain of 2.0% proof stress),  $\varepsilon_u$  (total strain corresponds to  $\sigma_u$ ), and  $\sigma_u$ .

$$a = \sigma_{2.0}(1 + \varepsilon_{2.0}) - b\varepsilon_{2.0} \tag{13}$$

$$b = \frac{\sigma_u(1 + \varepsilon_u) - \sigma_{2.0}(1 + \varepsilon_{2.0})}{\varepsilon_u - \varepsilon_{2.0}}$$
(14)

Besides the two-stage and multi-stage models based on the R-O expression, some updated models as transformations of the R-O expression or as combinations of the R-O expression and other equations have been proposed. MacDonald [17] came up with a uniform expression for modeling the full range  $\sigma$ - $\varepsilon$  relationship of cold-formed stainless steel as shown in Eq. (15).

$$\varepsilon = \frac{\sigma}{E} + 0.002 \left(\frac{\sigma}{\sigma_{0.2}}\right)^{i+j\left(\frac{\sigma}{\sigma_{0.2}}\right)^k} \quad \text{for } 0 \le \sigma \le \sigma_u$$
 (15)

The idea of this model is to amplify the value of n in Eq. (2) for the larger strain region, particularly after  $\sigma_{0.2}$ . The numerical coefficients i, j and k were obtained by error minimization on the test data. These coefficients were calculated as numbers between 2.5 and 6.0 and were found to be related to the steel sheet thickness.

Olsson [14] conducted research with a focus on plasticity models for stainless steel alloys and proposed a two-stage model depicting the relationship between the true stress  $\sigma^t = \sigma(1+\varepsilon)$  and engineering strain  $\varepsilon$ . Eq. (2) is used as the first stage expression when  $0 \le \sigma \le \sigma_{\varepsilon=0.02}$ , where  $\sigma_{\varepsilon=0.02}$  is the stress corresponding to  $\varepsilon=0.02$ . The second stage is depicted as a line when  $\sigma_{\varepsilon=0.02} < \sigma \le \sigma_u$ .

Abdella [18] proposed an approximate inversion of Eq. (2) and Eq. (6) for stainless steel alloys as shown in Eq. (16):

$$\sigma_{n} = \begin{cases} \frac{r\varepsilon_{n}}{1 + (r - 1)\varepsilon_{n}^{p}} & \text{for } 0 \le \varepsilon_{n} < 1\\ 1 + \frac{r_{0.2}(\varepsilon_{n} - 1)}{1 + (r^{*} - 1)\left(\frac{\varepsilon_{n} - 1}{\varepsilon_{nu}}\right)^{p^{*}}} & \text{for } 1 < \varepsilon_{n} \le \varepsilon_{nu} \end{cases}$$

$$(16)$$

where  $\sigma_n$  is the stress normalized by  $\sigma_{0,2}$ ,  $\varepsilon_n$  is the strain normalized by  $\varepsilon_{0,2}$ . All other parameters are clearly defined in [18]. The proposed explicit expressions were verified by fitting the  $\sigma$ - $\varepsilon$  curve database from [9].

Ma et al. [19] conducted a series of material properties experiments on cold-formed high strength steel with nominal yield strength up to 1100 MPa and proposed a new constitutive model based on the original R-O expression (i.e. Eq. (2)). The strain, as the output of the model, is explicitly depicted as expressions of plastic strain,  $\varepsilon_{pl}$ , as shown in Eq. (17):

$$\varepsilon = \varepsilon_p + \frac{\sigma}{E} = \varepsilon_p + \left(\frac{\sigma_{0.2}}{E}\right) \left(\frac{\varepsilon_p}{0.002}\right)^{\left(\frac{1}{n_0 + \kappa \varepsilon_p^m}\right)} \tag{17}$$

where K is determined per arithmetic consistency at the ultimate point as defined in [19].

Besides the stress-strain model itself, accurate prediction of the parameters required by the model is also essential. Gardner and Yun [20] collected  $\sigma$ - $\varepsilon$  curves of CFS sheets with nominal yield strengths ranging from 235 MPa to 1100 MPa from over 700 experiments. They reviewed the predictive equations for the key parameters of the two-stage CFS stress-strain model (e.g. model proposed by Mirambell and Real [8], Eqs. (2) and (3)) from existing literature and then developed a series of equations for these parameters based on the literature review and the statistical study on the collected experimental database. The

**Table 1** Chemical composition of AHSS.

Steel	DP-340	DP-580	DP-700	HSLA-700	MS-1030	MS-1200
C (max %)	0.12	0.167	0.17	0.104	0.16	0.28
Si (max %)	0.4	1.413	0.4	0.012	0.4	0.4
Mn (max %)	1.6	2	1.7	2.32	1.8	1.3
P (max %)	0.025	0.01	0.02	0.013	0.02	0.02
S (max %)	0.01	0.002	0.01	0.004	0.01	0.01
Al (%)	≥0.015	0.047	≥0.01	0.031	0.015	0.015
Nb + Ti (max %)	0.1	0.006	0.15	_	0.1	0.1
Cr + Mo (max %)	1	0.043	1	0.606	1	1
V (max %)	0.2	0.005	-	0.001	-	_
B (max %)	0.005	0.0003	0.005	0.0001	0.005	0.01
Cu (max %)	0.2	0.02	0.2	0.02	0.2	0.2
Ni (%)	-	0.01	-	0.01	-	_
Sn (%)	-	0.008	-	0.002	-	_
N (%)	-	0.004	-	0.005	-	_
Cb (%)	-	0.003	-	0.002	-	_
Sb (%)	-	-	-	0.001	-	_
Ca (%)	-	-		0.001	-	-

accuracy of the predictive equations was verified by comparison between the stress-strain model using parameters predicted by the proposed equations and parameters captured from the experimental database. Further discussion regarding the suitability of existing predictive parameters with the AHSS database are presented in Section 5.1.

## 3. Tensile coupon testing

#### 3.1. Test specimens

A total of 43 coupons were cut from 6 steel sheets by waterjet at UW-Madison TEAMLab and H&H Precision Wire in Newport, PA. The AHSS sheets including dual phase steel (DP) and martensitic steel (MS) with five different grades were studied. A piece of high-strength low-alloy steel (HSLA) (a type of conventional high-strength steel) sheet was also studied in this paper. The chemical composition of the tested steels is shown in Table 1. Note for DP-340, DP-700, and MS sheets, the composition is typical only, because exact chemical composition is proprietary. Nominal yield strengths range from 340 MPa to 1200 MPa and nominal ultimate strength range from 590 MPa to 1500 MPa. Nominal dimensions of the coupon are per ASTM E8 [4] as shown in Fig. 2. Each steel sheet was labeled by its steel family and nominal yield strength in MPa, i.e.: DP-340, DP-580, DP-700, HSLA-700, MS-1030, and MS-1200. The coupons were labeled by the steel sheet label, the cutting direction, and an index number. For example, HSLA-700L01 stands for coupon #1 cut along the longitudinal (coiling) direction of sheet HSLA-700. Other direction labels included "T" for transverse direction and "D" for diagonal (45°) direction along the sheet. Table 2 summarizes the nominal properties and test matrix. Actual width b and thickness t for each coupon was measured before the test using caliper and micrometer as reported in Table 3. HSLA-700 and DP-700 were coated by galvanized zinc and the actual thicknesses of these coupons were measured after removal of the coating by 1-M HCl solution, after which the thickness of the coupons reduced by 0.04 mm on average. The other steel sheets were uncoated.

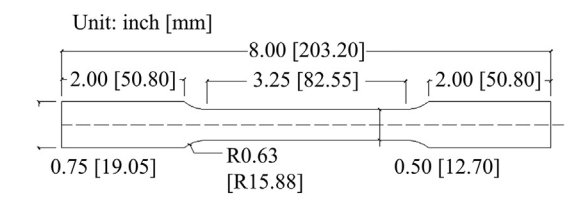


Fig. 2. Nominal dimensional tensile coupon test specimen.

**Table 2**Nominal coupon properties and test matrix.

Steel	t (mm)	$\sigma_y$ (MPa)	$\sigma_u$ (MPa)	Test matrix
DP-340	1.4	340	590	L:2, T:2, D:1
DP-580	1.8	580	980	L:5, T:4, D:0
DP-700	1.4	700	980	L:2, T:2, D:2
HSLA-700	0.6	700	980	L:5, T:3, D:0
MS-1030	1.0	1030	1300	L:4, T:2, D:2
MS-1200	1.0	1200	1500	L:3, T:2, D:2

#### 3.2. Test procedures

A MTS Criterion Model 43 loading system with a maximum capacity of 50 kN was used for the tensile tests. An extensometer with 25.4 mm gauge length was attached to the coupon center to measure strain. Before the test, the measured width b and thickness t of the coupon was input into the test control program, so that the real time relationship between engineering stress (applied load divided by the initial cross-sectional area of the reduced parallel section) and strain (extensometer reading) was available during the test. A previous study [21] has indicated some loading rate  $\sigma$ - $\varepsilon$  sensitivity. During the test, two different loading rates conforming to ASTM requirements [4] were used: initially, the loading rate was 0.2 mm/min until the stress achieved the nominal yield strength; the loading rate was then increased to 0.6 mm/min until

**Table 3**Properties of AHSS coupon specimens.

Series	t	b	Е	C	σ		σ.	C	σ.
361163	mm	mm	GPa	$\varepsilon_{0.2}$	$\sigma_{0.2}$ MPa	$\varepsilon_u$ %	$\sigma_u$ MPa	$\varepsilon_f$ %	$\sigma_{\!f}$ MPa
DP-340L01	1.382	12.76	215	0.38	378	15.2	608	22.1	601
DP-340L02	1.373	12.74	208	0.36	338	13.7	575	17.4	550
DP-340T01	1.378	12.74	213	0.37	357	10.8	598	11.9	581
DP-340T02	1.381	12.74	219	0.36	360	14.6	603	22.1	580
DP-340D01	1.390	12.75	203	0.38	365	14.2	595	16.4	580
DP-580L01	1.819	13.10	193	0.52	622	11.7	958	13.0	957
DP-580L03	1.818	13.03	197	0.52	626	11.8	945	20.0	902
DP-580L04	1.816	13.12	188	0.53	625	11.8	945	19.8	872
DP-580L13	1.810	12.96	191	0.53	636	9.1	954	16.2	907
DP-580L23	1.803	12.90	197	0.52	638	12.4	970	22.9	841
DP-580T01	1.817	13.07	198	0.52	634	10.2	953	12.4	940
DP-580T02	1.812	13.02	207	0.51	643	9.9	952	11.3	940
DP-580T03	1.802	13.04	209	0.51	640	9.2	962	11.3	922
DP-580T06	1.794	13.07	207	0.51	645	9.7	970	11.2	947
DP-700L01	1.399	12.63	208	0.55	725	7.5	950	16.4	654
DP-700L02	1.394	12.73	216	0.53	717	7.8	952	14.7	705
DP-700T01	1.422	12.61	223	0.50	659	6.7	951	13.7	812
DP-700T02	1.422	12.63	217	0.50	648	6.0	947	13.8	802
DP-700D01	1.410	12.72	227	0.50	681	5.8	937	9.4	826
DP-700D02	1.416	12.73	206	0.54	696	6.0	945	15.8	634
HSLA-700L02	0.620	12.25	175	0.62	732	7.8	1037	8.3	1032
HSLA-700L03	0.629	12.61	176	0.59	677	7.7	993	8.1	986
HSLA-700L04	0.626	12.60	219	0.52	709	5.1	1022	5.4	1014
HSLA-700L08	0.630	12.53	216	0.52	698	6.6	1004	7.7	980
HSLA-700L16	0.628	12.63	191	0.57	714	7.8	1072	9.5	1061
HSLA-700T02	0.619	12.60	199	0.54	677	6.8	1009	7.0	1007
HSLA-700T03	0.623	12.60	183	0.56	656	7.2	982	7.5	981
HSLA-700T11	0.616	12.63	198	0.55	689	7.8	1045	8.7	1035
MS-1030L01	1.000	12.73	225	0.77	1286	3.0	1380	5.6	978
MS-1030L02	1.006	12.73	214	0.77	1223	2.1	1306	3.1	1284
MS-1030L03	0.999	12.74	219	0.75	1199	2.6	1288	3.3	1252
MS-1030L04	1.002	12.73	216	0.76	1206	3.1	1304	3.4	1288
MS-1030T01	1.008	12.73	215	0.75	1173	2.6	1316	3.0	1291
MS-1030T02	1.007	12.77	226	0.72	1174	2.2	1326	2.4	1313
MS-1030D01	1.010	12.73	214	0.75	1185	2.1	1317	2.1	1307
MS-1030D02	1.011	12.73	211	0.76	1175	2.3	1313	6.9	844
MS-1200L01	1.008	12.80	205	0.84	1311	2.9	1490	6.5	1140
MS-1200L02	0.995	12.73	219	0.80	1322	2.9	1505	4.6	1462
MS-1200L03	0.997	12.76	199	0.85	1292	3.6	1490	3.9	1455
MS-1200T01	1.008	12.76	234	0.77	1324	3.4	1519	4.0	1491
MS-1200T02	1.004	12.78	216	0.79	1280	3.3	1471	3.9	1433
MS-1200D01	1.003	12.81	220	0.81	1337	3.8	1534	7.0	1230
MS-1200D02	1.008	12.79	215	0.80	1282	2.4	1460	5.7	1158

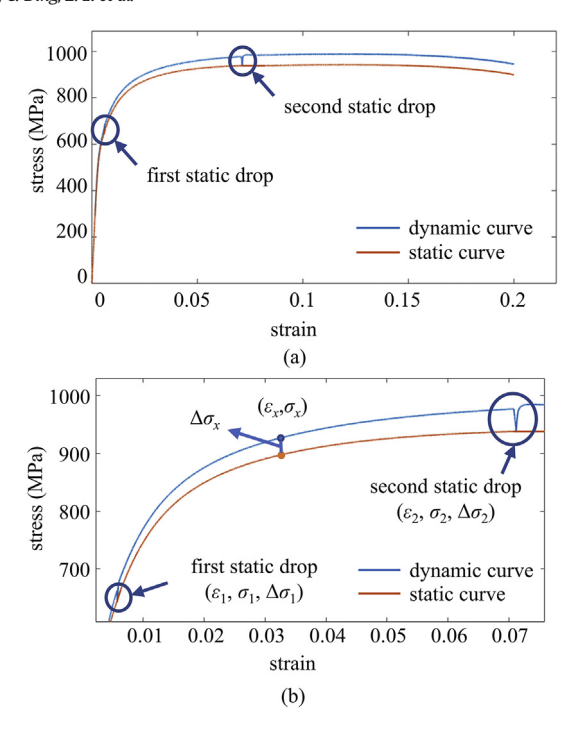


**Fig. 3.** (a) Comparison between dynamic and static  $\sigma$ - $\varepsilon$  curve; (b) (zoom-in view) conversion from dynamic stress to static stress.

fracture. Similar to the recommendation in [5], a slower loading rate before achieving the nominal yield strength was utilized to guarantee sufficient data in determining the elastic modulus. Consistent with Huang's recommendation [5], each test was manually paused twice. When the test was paused, the stress would decrease until stable and the duration for each pause was three minutes. For each test, the first pause was at the nominal yield strength and the second pause was at the nominal ultimate strength, as shown in Fig. 3(a). Pausing near the yield strength (0.2% proof stress) and ultimate strength for 100 s to allow the stress relaxation to take place is recommended by [5]. Prior to testing, only the nominal values of yield and ultimate strengths are known, therefore the nominal values were utilized for the generation of static drops. The static drop is used to estimate any stress amplification from loading rate and to calculate the static stress.

# 3.3. Test results

For each test, the primary result is the dynamic  $\sigma$ - $\varepsilon$  curve. Following the steps as depicted in Fig. 3, the static stress for each applicable data point is calculated by subtracting the stress amplification from its dynamic stress using the two static drops generated during the test, where  $\Delta \sigma_x$  is the stress amplification of location x. When x is between the proportional limit and the left end of the first static drop,  $\Delta \sigma_x$  is calculated by Eq. (18); when x is between the right end of the first static drop and the left end of the second static drop,  $\Delta \sigma_x$  is calculated by Eq. (19); when x is after the right end of the second static drop,  $\Delta \sigma_x$  is calculated by Eq. (20).

$$\Delta\sigma_{x} = \frac{\varepsilon_{x}\Delta\sigma_{1}}{\varepsilon_{1}} \tag{18}$$

$$\Delta\sigma_{x} = \frac{(\Delta\sigma_{2} - \Delta\sigma_{1}) \times (\varepsilon_{x} - \varepsilon_{1})}{\varepsilon_{2} - \varepsilon_{1}} + \Delta\sigma_{1} \tag{19}$$

$$\Delta \sigma_{x} = \Delta \sigma_{2} \tag{20}$$

When the loading is paused to generate the static drops, the strain increases slightly; when the loading is resumed, the stress rapidly

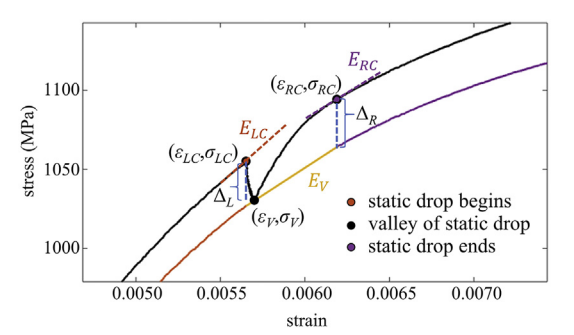


Fig. 4. V shape dynamic stress-strain relationship at static drops.

increases from the valley of static drop and continues along the original dynamic path. These processes generated a V shape dynamic stress-strain relationship as shown in Fig. 4.

A linear relationship is proposed and recommended to define the static stress-strain relationship for data within the V shape. First, the points where static drop begins and ends, as well as the valley of the V shape static drop are found manually. The linear relationship is assumed to pass through the valley and its slope is  $E_V$  as calculated by Eq. (21):

$$E_V = \tan \frac{\arctan E_{LC} + \arctan E_{RC}}{2} \tag{21}$$

where  $E_{LC}$  is the slope at the beginning (left) of the static drop and it is defined as the slope of linear regression for the ten data points before,  $E_{RC}$  is the slope at the end (right) of the static drop and it is defined as the slope of linear regression for the ten data points after.

The stress amplification at the beginning of the static drop,  $\Delta_L$ , is calculated by Eq. (22), and the stress amplification at the end of the static drop,  $\Delta_R$ , is calculated by Eq. (23):

$$\Delta_{L} = \sigma_{LC} - [E_{V}(\varepsilon_{LC} - \varepsilon_{V}) + \sigma_{V}]$$
 (22)

$$\Delta_{R} = \sigma_{RC} - [E_{V}(\varepsilon_{RC} - \varepsilon_{V}) + \sigma_{V}]$$
 (23)

where  $\varepsilon_{LC}$  and  $\sigma_{LC}$  are the strain and stress of static drop beginning,  $\varepsilon_{RC}$  and  $\sigma_{RC}$  are the strain and stress of static drop end,  $\varepsilon_{V}$  and  $\sigma_{V}$  are the strain and stress of static drop valley.

Note that for the first static drop, the loading rate was 0.2 mm/min until the pause, and changed to 0.6 mm/min when the loading resumed. Therefore, the difference between  $\Delta_L$  and  $\Delta_R$  of the first static drop might indicate the difference of stress amplification resulting from different loading rates. A faster loading rate will result in a slightly larger dynamic stress amplification (and hence slightly larger static drop), but regardless of the loading rate, the static drop will always reach the same level.

A summary of a representative static  $\sigma$ - $\varepsilon$  curve for each steel is shown in Fig. 5. To ensure each data point on the  $\sigma$ - $\varepsilon$  curve has the same weight, the experimental curve was represented by a generalized curve. Sadowski et al. [22] used a two-stage seventh order polynomial

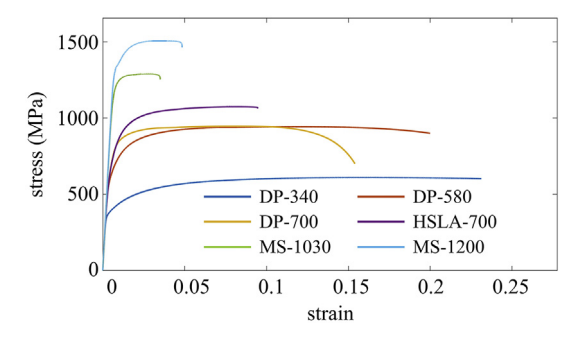


**Fig. 5.** Representative static σ-ε curve for each steel.

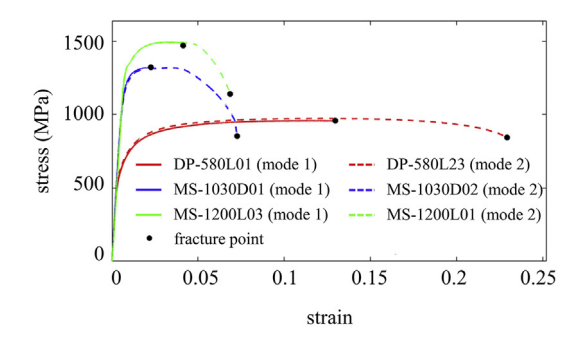


Fig. 6. Different strain hardening modes for DP-580, MS-1030 and MS-1200.

to represent the experimental curve. However, their polynomial model used strain as the model input and stress as the model output, which is the inverse of the R-O expression, and although the coefficient of variance between the polynomial and the experimental  $\sigma$ - $\varepsilon$  curve was larger than 0.96, some local differences were significant. To avoid these two issues, the experimental  $\sigma$ - $\varepsilon$  curve was constructed by linear interpolation along the stress axis with a uniform stress increment of 0.1 MPa.

Material properties including elastic modulus E, 0.2% proof stress  $\sigma_{0.2}$ , strain at 0.2% proof stress  $\varepsilon_{0.2}$ , ultimate strength  $\sigma_u$ , ultimate strain  $\varepsilon_u$ , fracture stress  $\sigma_f$ , and fracture strain  $\varepsilon_f$  were extracted from the static  $\sigma$ - $\varepsilon$  curves and are given in Table 3.

For E, the slope of the linear regression of all data points between stresses of 20% and 45% of the nominal yield strength was used [5]. The 0.2% offset point was determined as the point with a plastic strain of 0.002. The ultimate point was determined as the point with the largest static stress. The ratio of  $\sigma_u/\sigma_{0.2}$ , which is an indicator of curve nonlinearity, varies from 1.1 to 1.7. AHSS with lower nominal yield strength tends to have a larger  $\sigma_u/\sigma_{0.2}$ . The fracture strain was obtained as the strain prior to a considerable reduction of engineering stress from the real-time stress-strain relationship due to fracture of the specimen [5]. In addition, two different fracture modes are observed among the experimental AHSS  $\sigma$ - $\varepsilon$  curves and some examples are shown in Fig. 6. The first mode (mode 1) has a sudden fracture and the second mode (mode 2) has a gradual strain softening process. Different fracture modes affect the fracture point. In addition, there are generally no obvious effects of cutting directions on the material properties.

## 4. Updated two-stage plus linear stress-strain model

In this section, existing two-stage and multiple-stage stress-strain models discussed as in Section 2 were used to fit the AHSS  $\sigma$ - $\varepsilon$  curves from experiments as described in Section 3.3. Although some of the researchers provided predictive equations for essential parameters of their stress-strain model, the equations were derived from particular steel databases, which are different from AHSS in types, grades, and stress-strain behaviors. Therefore, to achieve optimal fit, the predictive expressions were not adopted in this section; rather, the required parameters of these models were fit from the AHSS experimental results. Optimal fit was achieved by maximizing the coefficient of determination ( $R^2$ ) between the experimental curve and the numerical model, as shown in Eq. (24):

$$R^2 = 1 - \frac{SS_{res}}{SS_{tot}} = 1 - \frac{\sum_{i} (\epsilon_i - \epsilon(\sigma_i))^2}{\sum_{i} (\epsilon_i - \overline{\epsilon}_i)^2}$$
 (24)

where  $\sigma_i$  and  $\varepsilon_i$  are the stress and strain of data point i of the experimental curve;  $\varepsilon(\sigma_i)$  is the model strain corresponding to  $\sigma_i$ ;  $\overline{\varepsilon}_i$  is the average of experimental strains.

Noticeably, for R-O models, the  $R^2$  is calculated by the difference of strain, rather than stress. Therefore, for higher strain ranges (e.g. the third stage of the three-stage model),  $R^2$  could be small (i.e. poor fit

between the test curve and the model), even if the difference between the test curve and the model is not obvious visually.

#### 4.1. Optimal fit between AHSS stress-strain curves and existing models

Optimal fit between experimental and existing models, using DP-700L02 as an example, are shown in Fig. 7. Models proposed by Mirambell [8] (Fig. 7(a)) and Rasmussen [9] (Fig. 7(b)) provide accurate fit for the first stage; while the strain model prediction is lower than experimental strain at the beginning of the second stage (starting from 0.2% proof stress). Additionally, neither of these two models mathematically pass through the ultimate point, the difference of the ultimate strain between the model prediction and the test data is obvious. The percentage difference for Mirambell's model ranges from 6.5% to 23.7% and for Rasmussen's model ranges from 12.4% to 47.4%. The inaccuracy of strain prediction on high stress range is large when applying Rasmussen's model, because the AHSS being studied in particular the MS, are less ductile than the stainless steel discussed in [9], and the approximation of using ultimate strain as the plastic strain of the ultimate point leads to an obvious inaccuracy.

Gardner's works [10,15] provide three formats of the updated second stage model (Eq. (6), Eq. (7), and Eq. (11)). As shown in Fig. 7(c), Eq. (6) mathematically ensures the model passes through the ultimate point, while similar to the case of Mirambell's model, the strain is underestimated at the beginning of the second stage. Eq. (7) provides excellent fit accuracy between 0.2% proof stress and 1.0% proof stress, while the fit after 1.0% proof stress is less accurate, particularly at high stress range.

The model proposed by Quach [13] (Fig. 7(d)) gives excellent fit for the first two stages, while the third stage by using Eq. (12) provides less accurate fit. Also, Quach's model requires three more parameters ( $\sigma_{1.0}$ ,  $\sigma_{2.0}$  and  $\varepsilon_{2.0}$ ) than Mirambell's and Rasmussen's model, which might limit the feasibility of the model. Hradil's three-stage model [12] (Fig. 7(e)) provides excellent fit accuracy for MS-1030 and MS-1200 along the full stress range. For DP and HSLA, the first two stages are excellently fitted, while the fit for the beginning of the third stage (Eq. (10)) is less accurate, particularly for DP-340. Also, Hradil's model requires more parameters ( $\sigma_{1.0}$  and an extra exponential coefficient for the third stage) than others' two-stage models. The accuracy of the fit can be increased if the number of model stages increases, however an increased number of extra parameters are also required (at least two extra parameters for each extra stage).

MacDonald's one-stage model with variable exponential coefficients [17] (Fig. 7(f)) provides an excellent fit up to  $\sigma_{0.2}$ , while the fit is less accurate for the higher stress range. More importantly, the model is particularly sensitive to the three parameters i, j, and K and no accurate predictive equations are available for these parameters. Therefore, the model is only applicable when the full experimental stress-strain data is available.

### 4.2. Updated stress-strain model

Based on the discussion above, the existing models might not be able to provide accurate fit for the AHSS stress-strain database, particularly for DP and HSLA steels. Although the existing models are able to accurately fit the AHSS test stress-strain curves up to around 0.2% proof stress for most cases, different levels of inaccuracies are commonly observed thereafter. Although the post-yield inaccuracies might not result in significant difference for many structural design and analysis cases, some other important scenarios can be sensitive to these inaccuracies. These scenarios include numerical simulations of steel forming, blast crushing, collapse, etc., where the relationship between local strain and engineering strain is crucial [23]. Therefore, a new model describing the stress-strain behavior of AHSS as shown in Fig. 8 is proposed. The proposed model is updated from Gardner's two-stage model (Eq. (2) and Eq. (6)), which passes through the origin, 0.2% proof stress, and

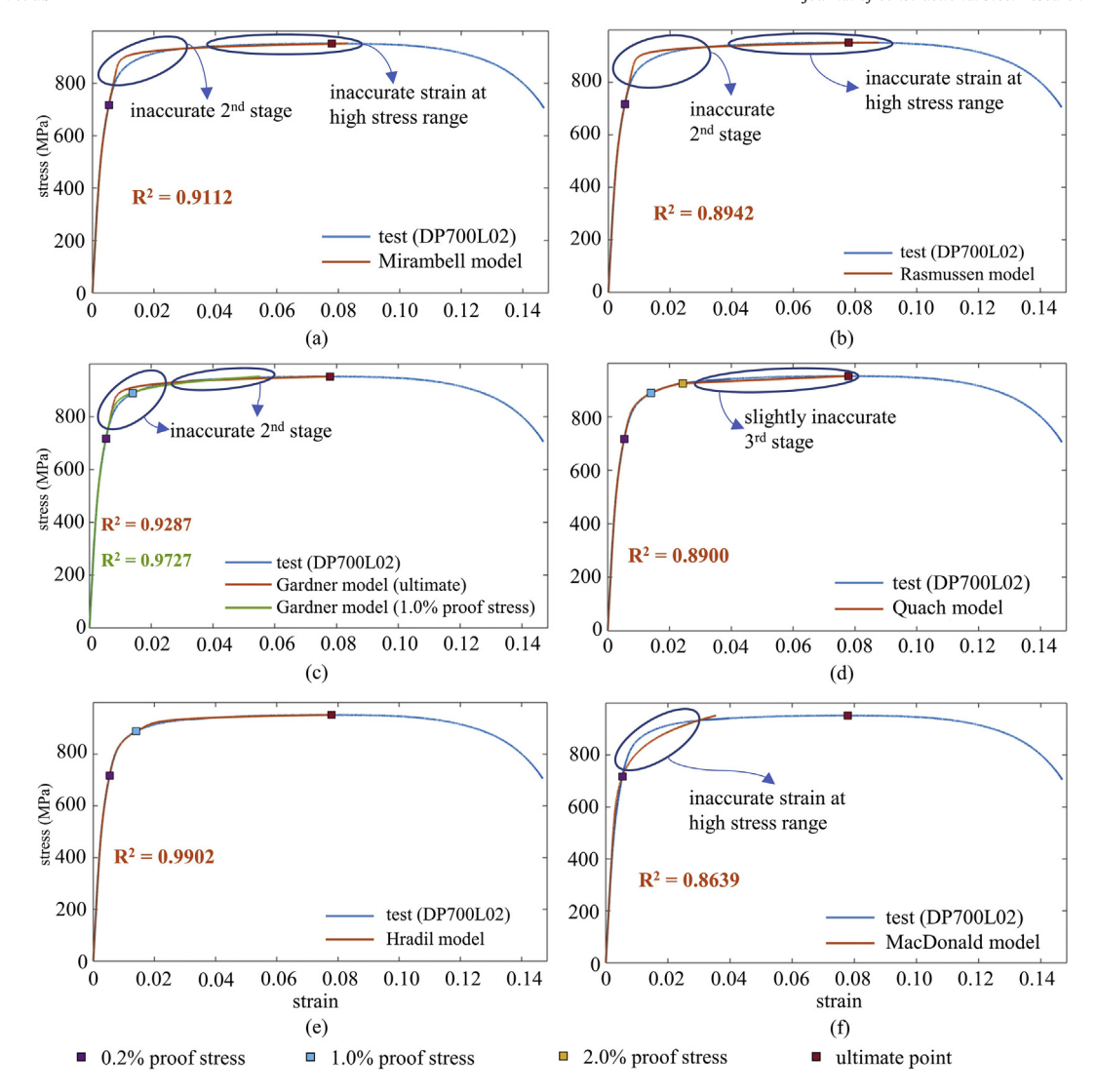


**Fig. 7.** Examples of fit between AHSS σ- $\varepsilon$  curves and existing models.

ends at the ultimate point. The expressions for the first stage and the second stage of the proposed stress-strain model are shown in Eq. (25):

$$\varepsilon = \begin{cases} \frac{\sigma}{E} + p \left(\frac{\sigma}{\sigma_p}\right)^n & \text{for } 0 \le \sigma \le \sigma_p \\ \frac{\sigma - \sigma_p}{E_p} + \left(\varepsilon_{eu} - \varepsilon_p - \frac{\sigma_{eu} - \sigma_p}{E_p}\right) \left(\frac{\sigma - \sigma_p}{\sigma_{eu} - \sigma_p}\right)^m + \varepsilon_p & \text{for } \sigma_p < \sigma \le \sigma_{eu} \end{cases}$$
(25)

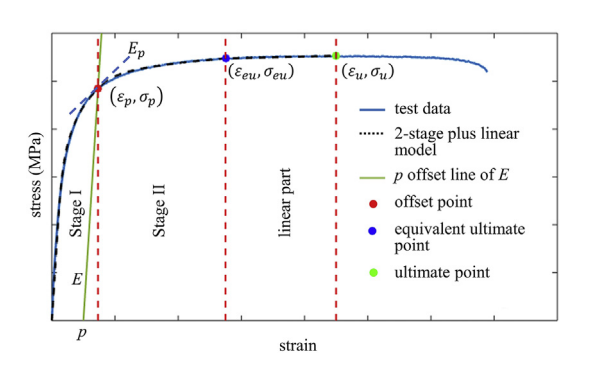


Fig. 8. Schematic diagram for the proposed two-stage plus linear model.

where  $\varepsilon_p$  and  $\sigma_p$  are the strain and stress of p offset (with a plastic strain of p);  $E_p$  is the tangent modulus at  $\sigma_p$  as calculated by Eq. (26);  $\varepsilon_{eu}$  and  $\sigma_{eu}$  are the strain and stress of the equivalent ultimate point.

$$\frac{1}{E_p} = \frac{\partial \varepsilon(\sigma)}{\partial \sigma} \bigg|_{\sigma = \sigma_p} = \frac{1 + pn \frac{\sigma}{\sigma_p^n} E}{E} \bigg|_{\sigma = \sigma} = \frac{1 + pn \frac{E}{\sigma_p}}{E} \Rightarrow E_p = \frac{E}{1 + pn \frac{E}{\sigma_p}}$$
(26)

Two major updates are made for the newly proposed model. The first update is to change the demarcation point (referred as *offset point* hereinafter) between the first and the second stage from 0.2% proof stress to a reassigned proof stress *p*. The second update is to change the end of the second stage from the ultimate point to *the equivalent ultimate point*.

The equivalent ultimate point is defined as the point with a stress equals to 99% of the ultimate strength at strain hardening stage. The first stage of the proposed model is adopted from the origin to the offset point and the second stage is adopted from the offset point to the equivalent ultimate point. The  $\sigma$ - $\varepsilon$  relationship from the equivalent ultimate point to the ultimate point is described as a line.

For the first update, from the discussion in Section 4.1, the existing two-stage models are not able to provide accurate fit at the beginning of the second stage. The inaccuracy is caused by the inaccurate calculation of tangent modulus  $E_{0.2}$  at the  $\sigma_{0.2}$ , and  $E_{0.2}$  is required in the second-stage expression (e.g. Eq. (6)).  $E_{0.2}$  is calculated by using the

first stage expression (Eq. (2)) because the second stage equation (Eq. (6)) is unknown before the determination of  $E_{0.2}$ . This compromise is only accurate when the transition between the first and the second stage is smooth. From the experimental  $\sigma$ - $\varepsilon$  relationship (e.g. Fig. 5), DP and HSLA steels curves are highly non-linear when the plastic strain is smaller than 0.005; MS steels curves are largely non-linear when the plastic strain is smaller than 0.002, while the nonlinearity tends to be small and stable when the plastic strain approaches 0.005. Therefore, to provide an accurate tangent modulus at the offset point, a larger plastic strain p is needed, particularly for the DP and HSLA steels. The proof stress offset p from 0.002 to 0.020 at an increment of 0.001 were iterated for each experimental  $\sigma$ - $\varepsilon$  curve to find the optimal fit with the optimal p by using the error minimization method. From the result shown in Fig. 9, it is found that the optimal p for DP and HSLA steels is larger than 0.005, while for MS steels it is less than 0.005. In addition, for each experimental  $\sigma$ - $\varepsilon$  curve, the optimal p has a positive correlation with increasing  $\sigma_u/\sigma_{0.2}$ . A predictive equation is proposed for the optimal p as shown in Eq. (27) (the black dashed line in Fig. 9), so that p can be predicted for AHSS of different grades when  $\sigma_u/\sigma_{0.2}$  is known.

$$p = \frac{4}{150} \left( \frac{\sigma_u}{\sigma_{0,2}} - 1 \right) \tag{27}$$

While the data presented in Fig. 9 shows a clear trend between the optimal proof stress offset p and the  $\sigma_u/\sigma_{0.2}$  ratio, there is a visible scatter in the data. For each steel, a total of five to nine coupons were tested. Due to inherent variability in the samples, the optimal p found using error minimization might not be the only feasible value of the proof stress offset. Therefore, a range of p values within the scatter for each material was considered and tested for fit accuracy by determining the  $R^2$  for all specimens. The range of p values for each material which fit all specimens with an  $R^2$  greater or equal to 0.995 was determined and is shown as the error bars in Fig. 9. The recommended values of the proof stress offset p for each material was chosen to reflect the trend of decreasing proof stress offset with increasing nominal strength from the range of applicable offset values and is given in Table 4.

The second update is inspired by the characteristic of the AHSS  $\sigma$ - $\varepsilon$  curve. Compared with other steels with rounded  $\sigma$ - $\varepsilon$  curve, AHSS  $\sigma$ - $\varepsilon$  curves have a long strain hardening process with almost no stress increase before the ultimate point. For example, from  $\sigma_{eu}$  to  $\sigma_{uv}$ , the average strain increases are 46% for DP-340, 70% for DP-580, 91% for DP-700, 54% for HSLA-700, 68% for MS-1030, and 47% for MS-1200. For existing two stage models as discussed in Section 2, the slope change rate for the second stage model is determined by the second derivative of the  $\sigma$ - $\varepsilon$  relationship as shown in Eq. (28), where all parameters are material properties except for m.

$$\frac{\partial^{2} \varepsilon(\sigma)}{\partial \sigma^{2}} = \frac{\left(\varepsilon_{u} - \varepsilon_{0.2} - \frac{\sigma_{u} - \sigma_{0.2}}{E_{0.2}}\right) m(m-1)}{\left(\sigma_{u} - \sigma_{0.2}\right)^{m}} \left(\sigma - \sigma_{0.2}\right)^{m-2} \tag{28}$$

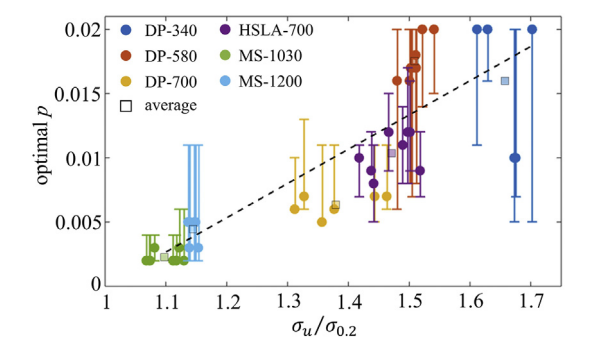


**Fig. 9.** The relationship between  $\sigma_u/\sigma_{0.2}$  and the optimal p.

**Table 4**Offset point, equivalent ultimate point and exponential coefficients for AHSS and HSLA steel

From the discussion on Fig. 1, for test curves with a long horizontal tail portion before the ultimate point (e.g. case n=1000), m will be dramatically increased for Fig. 1 to fit this tail. As a result, the increment of m will lower the model strain output and thus sacrifice the model fit accuracy at the beginning of the second stage. Therefore, to further improve the model accuracy, the long strain hardening tail portion with minimal stress increase before the ultimate point is excluded from the second stage model. The long horizontal tail portion is modeled with adequate accuracy and simplicity as a linear relationship between the equivalent ultimate point and the ultimate point.

Representative examples of the optimal fit with test data using the proposed two stage plus linear model for each steel are shown in Fig. 10. A summary of the average values of strain and stress at the offset point and the equivalent ultimate point as well as *n* and *m* determining the optimal fit for each material is shown in Table 4.

### 5. Predictive equations for model parameters

The  $\sigma$ - $\varepsilon$  relationship for the updated model requires seven material property parameters  $(E, \sigma_p, \varepsilon_p, \sigma_{eu}, \varepsilon_{eu}, \sigma_u, \text{ and } \varepsilon_u)$  and two non-property parameters (n and m). By definition,  $\varepsilon_p$  and  $\sigma_{eu}$  can be calculated by expressions  $\varepsilon_p = \sigma_p/E + p$  and  $\sigma_{eu} = 0.99\sigma_u$ . Therefore, seven parameters are needed to build the proposed model. Some of the the required parameters are not always provided in design code or from a steel manufacturer, and some are not always available from experiments for some cases. To enable the usability of the proposed model for these cases, the recommendations for these key parameters are provided.

#### 5.1. Predictive equations for model parameters from literature

Among the unknown parameters, some are commonly required by existing stress-strain models, which include elastic modulus, ultimate strength, and ultimate strain. Therefore, predictive equations of these parameters were used to fit the test results of AHSS and HSLA steel. Gardner and Yun [20] adopted the Mirambell and Real model [8] and developed predictive equations and numerical values for required model parameters after conducting a statistical study on CFS database. Fig. 11 shows two examples of different situations (cases 1, 2, and 3 from [20]) for the Mirambell and Real model [8] built by parameters from test results and the predictive equations developed in [20]. The first example on conventional CFS, shown in Fig. 11(a), is from a tensile test on 3.0 mm thick G450 specimen [24]. When using all parameters from the test (case 1), the 2-stage model [8] is able to provide accurate fit with the experimental curve. When using E,  $\sigma_{0.2}$ , and  $\sigma_u$  from the test, while using the rest parameters predicted by the proposed equations (case 2) to build the 2-stage model, the fit is generally accurate except at the high stress range approaching  $\sigma_u$ . When only  $\sigma_{0,2}$  is available from the test and all other required parameters are calculated by the proposed equations (case 3) to build the the 2-stage model, the model fit is inaccurate after passing through  $\sigma_{0.2}$ . The second example (Fig. 11(b)) shows an experimental  $\sigma$ - $\varepsilon$  curve from the AHSS database (DP580-L01). For case 1, as discussed in Section 4.1, the 2-stage model

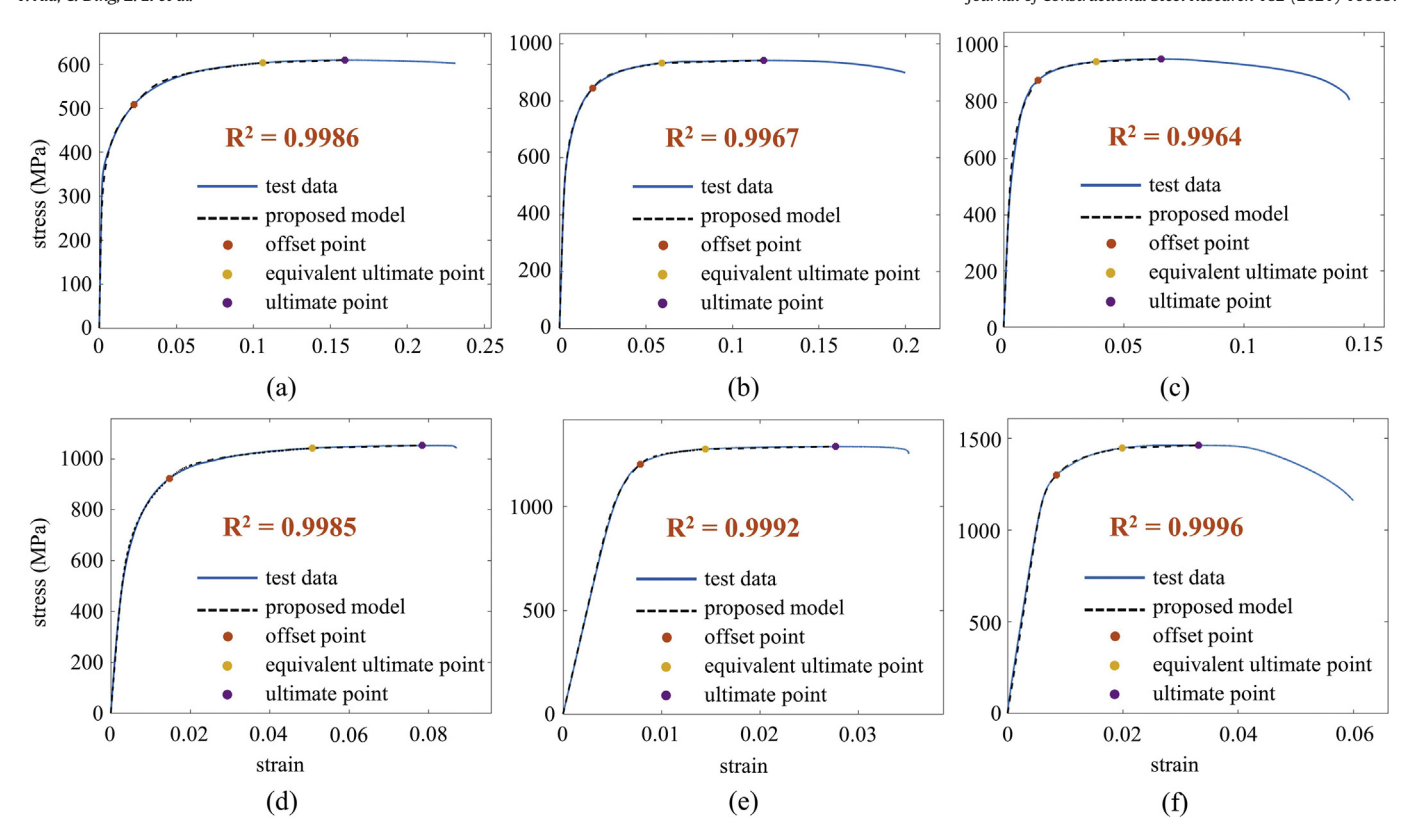


Fig. 10. Representative examples of the optimal fit with the experimental σ-ε curves using the proposed two-stage plus linear model for (a) DP-340; (b) DP-580; (c) DP-700; (d) HSLA-700; (e) MS-1030; (f) MS-1200.

built by parameters from the test can fit well for the first stage, while the beginning of the second stage is not accurately fitted. For case 2 and case 3, the first stage is well fitted, while the fit for the second stage is inaccurate. Similar to this example, the situations of different cases for DP-340, DP-580, DP-700, and HSLA-700 are similar. For MS steels,

600 zoom-in of region from 0.2% to 1.2% strain range 500 400 300 200 test data case 1: 2-stage model using E,  $\sigma_{0.2},\,\sigma_{\rm u},\,\varepsilon_{\rm u},\,n,$  and m from test 100 case 2: 2-stage model using E,  $\sigma_{0.2}$ , and  $\sigma_{0.0}$  from test case 3: 2-stage model using  $\sigma_{0.2}$  from test 0.005 0.01 0.015 0.02 0.025 (a) 1000 800 stress (MPa) case 1: 2-stage model using E,  $\sigma_{0.2}$ ,  $\sigma_{\rm u}$ ,  $\varepsilon_{\rm u}$ , n, and m from test 200 case 2: 2-stage model using  $E, \, \sigma_{0.2}, \, {\rm and} \, \sigma_{\rm u}$  from test case 3: 2-stage model using  $\sigma_{0.2}$  from test 0 0.05 0.15 strain (b)

**Fig. 11.** Examples of comparisons between stress-strain model [8] constructed by parameters from test and predicted parameters [20] for (a) conventional CFS (G450 steel from [24]) and (b) AHSS (DP-580L01).

although the fits for case 2 and case 3 are still not accurate, the inaccuracy is slightly smaller than that of DP or HSLA steel.

From Gardner and Yun's paper [20], the fit range for exponential coefficients *n* and *m* are different from the range of the proposed model. For the conventional 2-stage model, *n* determines the curvature from the origin to  $\sigma_{0.2}$ , and m determines the curvature from  $\sigma_{0.2}$  to  $\sigma_{u}$ . For the proposed 2-stage plus linear model, *n* determines the curvature from the origin to  $\sigma_n$ , and m determines the curvature from  $\sigma_n$  to  $\sigma_{eu}$ . Therefore, the predictive equations for *n* and *m* of existing two-stage models are not applicable for n and m of the proposed model. The average E of the tested AHSS sheets, as discussed in Section 3.3, is 208.0 GPa with a coefficient of variance of 0.065. Gardner and Yun's paper [20] and the AISI-S100 standard for cold-formed steel [25] recommends 203 GPa for E, which is only 2% lower than the test results. Therefore, E = 203GPa is recommended for AHSS in this paper when the test result is unavailable. A linear relationship between  $\varepsilon_u$  and  $\sigma_{0,2}/\sigma_u$  is proposed for both hot-rolled steel and CFS sheets, and its fit with AHSS results is shown in Fig. 12 [20]. From the figure, the predicted  $\varepsilon_u$  is 34% to 261% higher than the results from the tests.

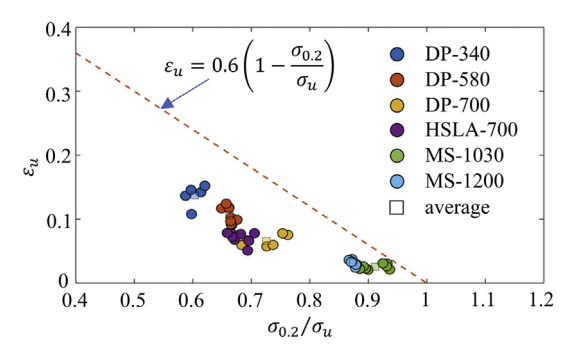


**Fig. 12.** Comparison of  $\varepsilon_u$  between prediction [20] and AHSS test data.

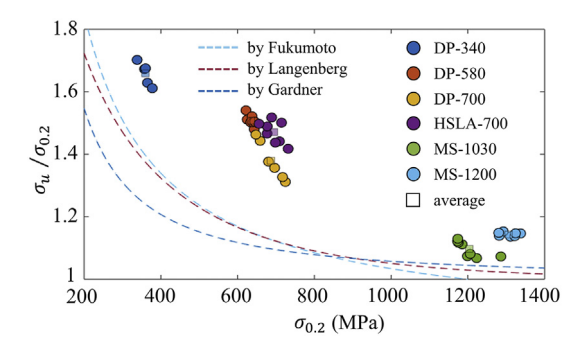


**Fig. 13.** Comparison of  $\sigma_u/\sigma_{0.2}$  between prediction [20,26,27] and AHSS test data.

For  $\sigma_u$ , the relationship between  $\sigma_u/\sigma_{0.2}$  and  $\sigma_{0.2}$  with three different expressions proposed by Fukumoto [26] (Eq. (29)), Langenberg [27] (Eq. (30)), and Gardner [20] (Eq. (31)) were compared.

$$\sigma_u/\sigma_{0.2} = 0.83 + 203.8/\sigma_{0.2} \tag{29}$$

$$\sigma_u/\sigma_{0.2} = \left[1 - 0.72e^{-0.0027\sigma_{0.2}}\right]^{-1} \tag{30}$$

$$\sigma_u/\sigma_{0.2} = 1 + (130/\sigma_{0.2})^{1.4}$$
 (31)

The fit with AHSS and HSLA steel curves is shown in Fig. 13. It was found the predicted  $\sigma_u/\sigma_{0.2}$  is largely conservative compared with tests results. Predicted  $\sigma_u$  can be calculated by the product of  $\sigma_u/\sigma_{0.2}$  and  $\sigma_{0.2}$ . The ultimate strength  $\sigma_u$  calculated by Eq. (29) and Eq. (30) is up to 26% less than the test results, while 28% less when using Eq. (31).

From the discussion above, the predictive equations from literature might not able to reasonably predict  $\varepsilon_u$  and  $\sigma_u$  of the AHSS database. Therefore, predictive equations for key parameters, excluding E, required by the proposed two-stage plus linear model need to be provided.

# 5.2. Expressions for material-property parameters

The predictive equations for material-property parameters required by the proposed two-stage plus linear model are provided based on a known 0.2% proof stress  $\sigma_{0.2}$ , which is typically available from a low strain level test or directly provided by the steel manufacturer. The relationship between  $\sigma_p$  and  $\sigma_{0.2}$  is plotted in Fig. 14. Test data for different steels are plotted as circles with different colors; additionally, the average of each steel is plotted as a square with the corresponding color. The plot suggests a strong linear relationship between  $\sigma_p$  and  $\sigma_{0.2}$  and therefore a linear expression in MPa as shown in Eq. (32) is fitted to describe the relationship.

$$\sigma_p = \begin{cases} 1.23 \times \sigma_{0.2} + 60 & \text{ for DP and HSLA} \\ \sigma_{0.2} & \text{ for MS} \end{cases} \tag{32}$$

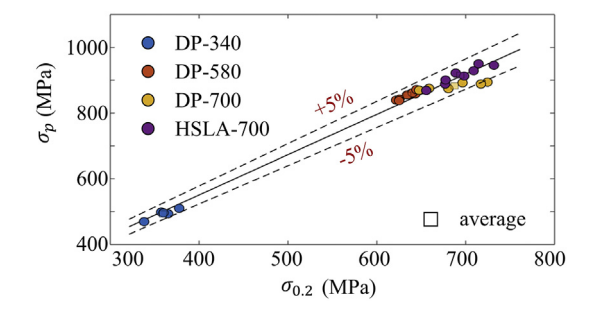
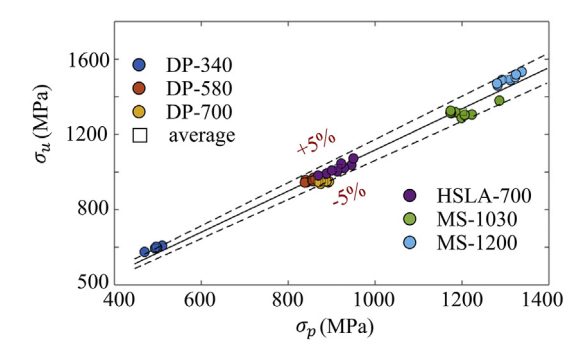


Fig. 14. Predictive expression for selected proof stress  $\sigma_p$  for AHSS when measured 0.2% proof stress  $\sigma_{0.2}$  is available.



**Fig. 15.** Predictive expression for ultimate strength  $\sigma_v$ .

Two trendlines with  $\pm 5\%$  variance is added to the plot and most of the test data is between the trendlines, which indicates a good accuracy of the expression. The maximum error between the predictive  $\sigma_p$  by Eq. (32) and the test data is 6.1%. It is recommended to use p=0.002 for MS steels, therefore  $\sigma_p=\sigma_{0.2}$ .

The relationship between  $\sigma_u$  and  $\sigma_p$  extracted from test data is plotted in Fig. 15. The plot indicates a strong linear relationship between the two parameters and a linear expression in MPa is fitted to the test data as shown in Eq. (33).

$$\sigma_u = 1.09 \times \sigma_p + 24 \tag{33}$$

Most test data is within the two trendlines with  $\pm 5\%$  variance for Eq. (33). For the case that  $\sigma_p$  is not available directly,  $\sigma_p$  is calculated by Eq. (32) firstly and then  $\sigma_u$  is calculated by Eq. (33). In this case, the difference of  $\sigma_u$  between predicted value and experimental data is less than 5% except DP-700; the difference for DP-700 is less than 10%.

The relationship between  $\varepsilon_u$  and  $\sigma_p/E$  is plotted in Fig. 16. As discussed in Section 3.3 and Section 4, even for the same type of steel with same cutting direction,  $\varepsilon_u$  may vary significantly because of the stress plateau near the ultimate point. Therefore, the relationship between  $\varepsilon_u$  and  $\sigma_p/E$  is not as clear as the two aforementioned stress expressions, while still sufficiently visible. For the four steels with nominal yield strength less than 1000 MPa, the ultimate strain decreases when  $\sigma_p/E$  increases; for MS-1030 and MS-1200, the ultimate strain is generally stable. Therefore, a two-part predictive expression as shown in Eq. (34) is fitted to the data.

$$\varepsilon_{u} = \begin{cases} -\frac{130}{3} \times \frac{\sigma_{p}}{E} + \frac{161}{600} & \text{for DP and HSLA} \\ 0.03 & \text{for MS} \end{cases}$$
 (34)

To include the relatively large variance of the ultimate strain, two trendlines with  $\pm$  40% variance is plotted and most test data is between these two trendlines. This large difference tolerance is also commonly used for the predictive expression for ultimate strain of stainless steel

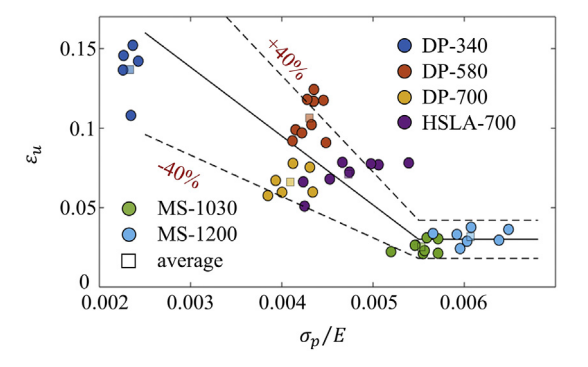


**Fig. 16.** Predictive expression for ultimate strain  $\varepsilon_u$ .

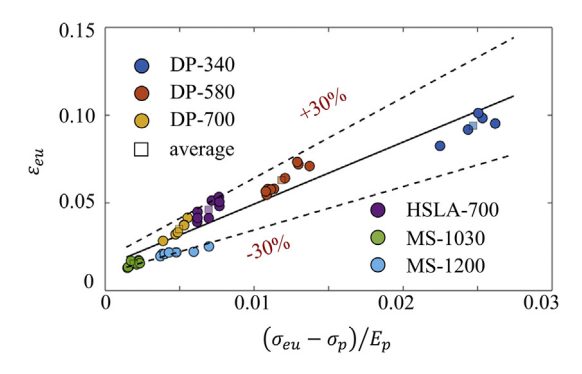


**Fig. 17.** Predictive expression for strain of the equivalent ultimate point  $\varepsilon_{ev}$ .

[9] and conventional CFS [20,28]. The difference between the predictive expression and the average of the test data is less than 20%.

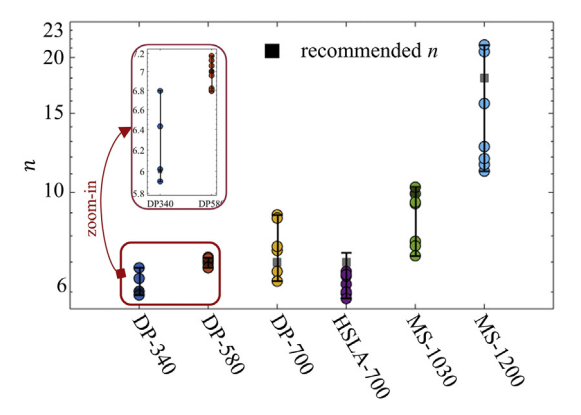
The relationship between  $\varepsilon_{eu}$  and  $(\sigma_{eu} - \sigma_p)/E_p$  is plotted in Fig. 17.  $E_p$  is the tangent modulus at  $\sigma_p$  and it is calculated by Eq. (26). A linear relationship is found and the line of best fit is closely approximated by Eq. (35).

$$\varepsilon_{eu} = 3.54 \times \frac{\sigma_{eu} - \sigma_p}{E_p} + 0.014 \tag{35}$$

Two trendlines with  $\pm$  30% variance with Eq. (35) is added to the plot in Fig. 17 and most of the test data lies between the trendlines. Similar to the case of ultimate strain, the difference between the predictive expression and the corresponding average value of strains of equivalent ultimate points from the experiment for each steel is less than 20%.

## 5.3. Recommendation for exponential coefficients n and m

As discussed in Section 2 (Fig. 1), the non-material property exponential coefficients n and m determine the degree of curvature for the first and second stage of the model, respectively, as described by Eq. (25). The values for n and m shown in Table 4 are determined by error minimization. A summary of n for each test is shown in Fig. 18. Based on the observation of  $\sigma$ - $\varepsilon$  curves for different type of steels (e.g. Fig. 5), the degree of curvature for the first stage, n, generally increases when the yield strength of steel increases. For example, the curve transition from the end of linear elastic region to the selected offset point for DP-340 is relatively gradual, while for the two MS steels is relatively sharp. This observation is supported by the error minimization fitting of n shown in Fig. 18 which indicates an overall trend that n increases as the steel strength increases. Due to the obvious scatter in the plot, instead of a continuous expression, a tabular recommendation of n for



 $\textbf{Fig. 18.} \ Recommendation for first stage exponential coefficient } n \ based on statistics study of experiment results.$ 

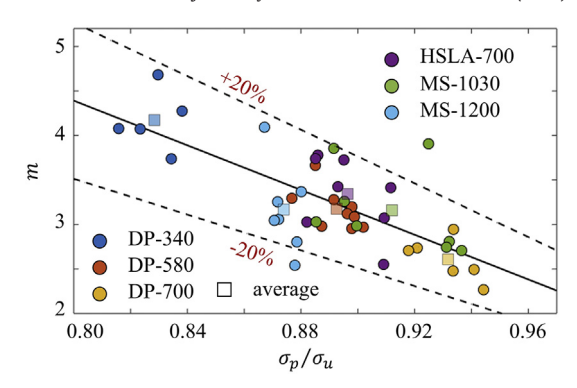


**Fig. 19.** Predictive equation for second stage exponential coefficient *m*.

each steel is proposed as shown by the black solid squares in Fig. 18 as the average approximation of the test data.

Similarly, m depicts the degree of the curvature for the second stage of the model from  $\sigma_p$  to  $\sigma_{eu}$ . Therefore, a relationship exists between m and  $\sigma_p/\sigma_u$  as plotted in Fig. 19. A linear relationship is observed and a linear expression given in Eq. (36) is fitted to the test data.

$$m = -12.55 \times \frac{\sigma_p}{\sigma_u} + 14.43 \tag{36}$$

Most m data is within  $\pm$  20% variance trendlines of Eq. (36); while the difference between Eq. (36) and the average of the test data given in Table 4 is less than 10%.

#### 6. Yield strength determination

In conventional CFS numerical modeling, the 0.2% proof stress  $\sigma_{0.2}$  is widely considered as yield strength and used as the offset point for existing stress-strain models as described in Section 2. From the discussion in Section 4, using  $\sigma_{0.2}$  as the offset point is not able to accurately fit the AHSS experimental stress-strain database. Instead, using the recommended p proof stress as the offset point is proposed for its excellent fit with the database. Additionally, as shown in Table 4, the ratio between  $\sigma_u$  and  $\sigma_p$  is 1.1 for almost all AHSS and HSLA steel; the only exception is DP-340 where its ratio is 1.2. The value of this ratio is close to the ratio of  $\sigma_u/\sigma_{0.2}$  for most conventional CFS [20]. Therefore, the applicability of using the recommended p proof stress to represent the yield strength is investigated.

In this section, the energy method was used to verify the rationality of defining the yield strength using the recommended p proof stress. The area under the load-displacement curve from the origin to the fracture point is the dissipated energy during the whole loading process. From the definition of engineering strain and engineering stress, the area under the engineering  $\sigma$ - $\varepsilon$  curve is proportional to the dissipated energy, hence it will be called equivalent energy dissipation. If the areas under any two  $\sigma$ - $\varepsilon$  curves are equal, the energy dissipation of these two loading processes are equal. The equivalent energy dissipation for each experimental  $\sigma$ - $\varepsilon$  curve was calculated by the area under the curve. The equivalent energy dissipation for conventional steel stress-strain models was set equal to that of the experiment, and then the corresponding yield strength  $\sigma_{v}$  for these models was calculated. The calculated yield strength of each conventional model was compared with the conventional 0.2% proof stress  $\sigma_{0.2}$  and recommended p proof stress  $\sigma_p$  from Table 4. Additionally, when adopting  $\sigma_v = \sigma_p$  in the conventional models, the differences of the equivalent energy dissipation between conventional models and experimental  $\sigma$ - $\varepsilon$  curves were discussed.

The area  $S_0$  under the experimental  $\sigma$ - $\varepsilon$  curve from the origin to the fracture point for each specimen is calculated by trapezoidal numerical integration. Two conventional steel stress-strain models, the elastic

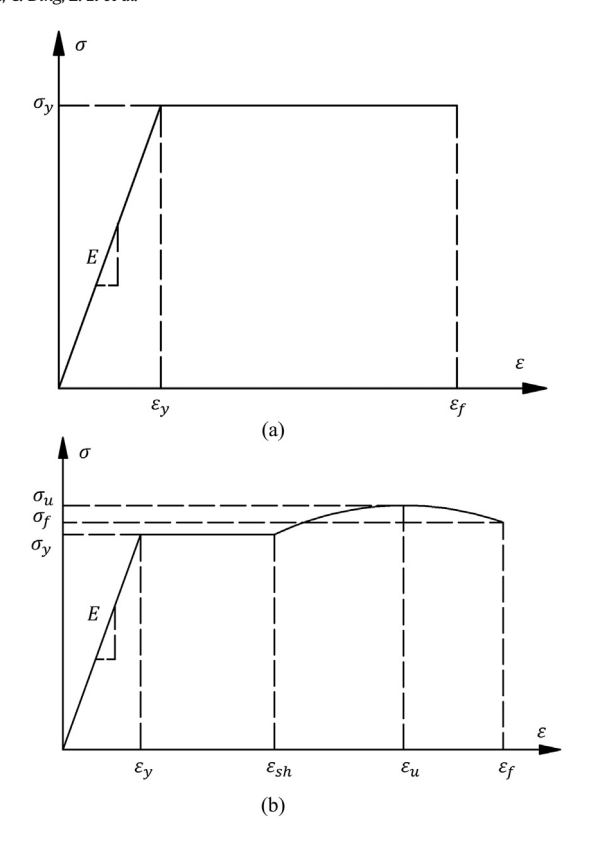


Fig. 20. The schematic diagram for (a) the EPP model and (b) the AEP model (bottom).

perfect plastic model (referred as EPP model hereinafter) and the artificial elastic plastic model with strain hardening and softening (referred as AEP model hereinafter) [29], are used in this section. Schematic diagrams of the EPP and AEP models are shown in Fig. 20. Most required parameters are determined from the experimental  $\sigma$ - $\varepsilon$  curves, including elastic modulus E, ultimate strain  $\varepsilon_u$ , ultimate strength  $\sigma_u$ , fracture strain  $\varepsilon_f$ , and fracture stress  $\sigma_f$ . The yield strength  $\sigma_y$  and the yield strain  $\varepsilon_y$  of both EPP and AEP model are the unknown material-property parameters to be determined.

The area  $S_1$  under the EPP model is calculated by Eq. (37).

$$\begin{split} S_1 &= \int_0^{\varepsilon_f} \sigma(\varepsilon) d\varepsilon = \frac{1}{2} \times \frac{\sigma_y}{E} \times \sigma_y + \sigma_y \times \left(\varepsilon_f - \frac{\sigma_y}{E}\right) \\ &= \left(\varepsilon_f - \frac{\sigma_y}{2E}\right) \times \sigma_y \end{split} \tag{37}$$

By assuming an equal energy dissipation between the experimental curve and the EPP model,  $\sigma_y$  is calculated by solving  $S_1 = S_0$  as shown in Eq. (38).

$$\sigma_{y} = E\varepsilon_{f} - \sqrt{\left(E\varepsilon_{f}\right)^{2} - 2ES_{0}}$$
(38)

The calculated  $\sigma_y$  is located on the experimental  $\sigma$ - $\varepsilon$  curve, and its corresponding offset  $p_{EPP}=\varepsilon_y-\sigma_y/E$  is calculated. The  $p_{EPP}$  values are averaged across each steel and are given in Table 5. The calculated  $p_{EPP}$  value is significantly larger than the traditional 0.2% and greater than the recommended offset p given in Table 4. The average percentage difference  $\Delta\sigma_{0.2EEP}$  between the calculated  $\sigma_y$  and  $\sigma_{0.2}$  from the test as well as the average percentage difference  $\Delta\sigma_{pEEP}$  between the calculated  $\sigma_y$  and the recommended proof stress  $\sigma_p$  from the test as determined in Section 4.2 are calculated and shown in Table 5. Overall,  $\sigma_y$  from the EPP model is closer to  $\sigma_p$  than  $\sigma_{0.2}$  for DP and HSLA steels, while  $\sigma_{0.2}$  is adopted as  $\sigma_p$  for MS steels. This shows that the recommended offset proof stress  $\sigma_p$  determined in Section 4.2 is a better fit to represent

**Table 5**Comparison among AHSS test curves, EPP model, and AEP model.

Steel	DP-340	DP-580	DP-700	HSLA-700	MS-1030	MS-1200
p <sub>EPP</sub> (%)	4.8	3.3	1.5	1.9	0.5	0.8
$\Delta\sigma_{0.2EPP}$ (%)	-35.8	-30.9	-24.4	-28.4	-5.0	-9.0
$\Delta\sigma_{pEPP}$ (%)	-11.9	-7.0	-2.9	-5.7	-5.0	-9.0
$\Delta S_{EPP}$ (%)	-11.8	-6.9	-2.9	-5.5	-4.5	-8.4
$p_{AEP}$ (%)	1.8	1.5	1.3	0.8	0.2	0.6
$\Delta\sigma_{0.2AEP}$ (%)	-23.0	-25.9	-26.4	-22.0	-1.0	-3.7
$\Delta\sigma_{pAEP}$ (%)	2.5	-0.2	-2.9	2.7	-1.0	-3.7
$\Delta S_{AEP}$ (%)	1.5	-0.0	-1.6	0.9	-0.5	-1.2
λ	6	6	4	4	2	2

the yield strength for the DP and HSLA steels than the traditional 0.2% proof stress.

For the AEP model, at the position where the yield plateau ends and the nonlinear strain hardening starts,  $\varepsilon_{sh}$ , is not clearly defined quantitatively. In this paper,  $\varepsilon_{sh}$  was initially determined by the statistical result of  $\lambda = \varepsilon_{sh}/\varepsilon_y$  for CFS specimens with a similar  $\sigma$ - $\varepsilon$  curve shape as the AEP model from previous studies. From Rogers's report [30], three specimens, 060-G300-SCDR3, 060-G300-SCL2, and 060-G300-SCT3 are applicable and their  $\lambda$  values are 6.70, 6.98 and 9.40 respectively. From Abdel's paper [31], specimens A-9 and B-4 are applicable and their  $\lambda$  values are 3.68 and 7.40 respectively. From Huang's paper [5], specimens AF-R1 and GF-R1 are applicable and their  $\lambda$  values are 2.50 and 4.20 respectively. The average value of  $\lambda$  is 5.84. Based on this data,  $\lambda$  in the AEP model is initially assumed as 6, an approximation of this average.

No mathematical model is specified in literature for the strain hardening and strain softening regions. In this study, a quadratic model  $\sigma(\varepsilon)$  $= a\varepsilon^2 + b\varepsilon + c$  for  $\varepsilon_{sh} \le \varepsilon \le \varepsilon_f$  is used. The values of  $\varepsilon_u$ ,  $\sigma_u$ ,  $\varepsilon_f$ , and  $\sigma_f$  from the experimental  $\sigma$ - $\varepsilon$  curves are used to build the AEP model, and  $\sigma_y$  is the only unknown parameter to be determined. The coefficients a, b, and c were solved by Eq. (39), Eq. (40), and Eq. (41) which are expressions of  $\sigma_y$ .

$$a = \frac{\varepsilon_{sh}(\sigma_f - \sigma_u) + \varepsilon_u(\sigma_y - \sigma_f) + \varepsilon_f(\sigma_u - \sigma_y)}{(\varepsilon_{sh} - \varepsilon_f)(\varepsilon_u - \varepsilon_{sh})(\varepsilon_f - \varepsilon_u)}$$
(39)

$$b = -\frac{\varepsilon_{sh}^{2}(\sigma_{f} - \sigma_{u}) + \varepsilon_{u}^{2}(\sigma_{y} - \sigma_{f}) + \varepsilon_{f}^{2}(\sigma_{u} - \sigma_{y})}{(\varepsilon_{sh} - \varepsilon_{f})(\varepsilon_{u} - \varepsilon_{sh})(\varepsilon_{f} - \varepsilon_{u})}$$
(40)

$$c = -\frac{\varepsilon_{sh}\varepsilon_{u}\sigma_{f}(\varepsilon_{u} - \varepsilon_{sh}) + \varepsilon_{sh}\varepsilon_{f}\sigma_{u}(\varepsilon_{sh} - \varepsilon_{f}) + \varepsilon_{u}\varepsilon_{f}\sigma_{y}(\varepsilon_{f} - \varepsilon_{u})}{(\varepsilon_{sh} - \varepsilon_{f})(\varepsilon_{u} - \varepsilon_{sh})(\varepsilon_{f} - \varepsilon_{u})}$$
(41)

Noticeably, by combining  $\sigma_y = a\varepsilon_{sh}^2 + b\varepsilon_{sh} + c$ ,  $\sigma_u = a\varepsilon_u^2 + b\varepsilon_u + c$ , and  $\sigma_f = a\varepsilon_f^2 + b\varepsilon_f + c$ , three constraints are generated and they are sufficient to solve a, b, and c as a set of unique solutions. By definition,  $\sigma_u$  is the peak of the strain hardening process, and likewise should be the peak of the quadratic model. Therefore, the percentage difference between the peak of the quadratic model and the ultimate strength,  $\delta_{peak}$ , is calculated, and if it is less than 1%, then the solution is considered valid. After the calculation of a, b, and c as expressions of  $\sigma_y$ , the area  $S_2$  under the AEP model is calculated as an expression of  $\sigma_y$  as shown in Eq. (42).

$$S_2 = \int_0^{\varepsilon_f} \sigma(\varepsilon) d\varepsilon = \left(\lambda - \frac{1}{2}\right) \frac{\sigma_y^2}{E} + \int_{\varepsilon_{\text{sh}}}^{\varepsilon_f} a\varepsilon^2 + b\varepsilon + cd\varepsilon \tag{42}$$

The yield strength  $\sigma_y$  is then calculated by solving  $S_0=S_2$  using the generalized reduced gradient nonlinear algorithm in Excel Solver and  $\delta_{peak}$  is then checked if it is within the 1% tolerance. Applying the initial  $\lambda$  for DP-340 and DP-580 gives very small  $\delta_{peak}$ . For DP-700, HSLA-700, MS-1030, and MS-1200,  $\delta_{peak}$  is larger than 10%. The major cause is, for these cases, a is significantly larger than that of DP-340 and DP-580. The

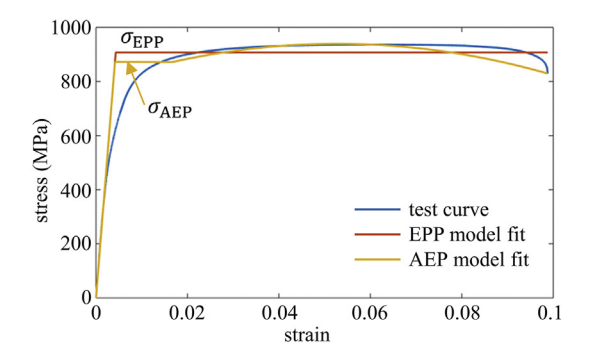


Fig. 21. EPP and AEP model based on test curve (DP-700D01).

references [5,30,31] used to calculate the initial  $\lambda$  only covered conventional grade steels, instead of high-strength steels. Good fits were achieved by varying  $\lambda$  and it was determined to use  $\lambda=6$  for DP-340 and DP-580,  $\lambda=4$  for DP-700 and HSLA-700, and  $\lambda=2$  for MS-1030 and MS-1200. The adjusted  $\lambda$  for each steel is inversely correlated to its nominal yield strength.

By using the adjusted  $\lambda$  for the AEP model,  $\sigma_y$  is calculated and then located on the experimental  $\sigma$ - $\varepsilon$  curve, and its corresponding offset  $p_{AEP} = \varepsilon_y - \sigma_y/E$  is calculated. The  $p_{AEP}$  values are averaged across each steel and are shown in Table 5. For DP and HSLA steels,  $p_{AEP}$  is significantly larger than 0.2%, while it is close to the recommended p given in Table 4, and for MS steels,  $p_{AEP}$  is slightly larger than the recommended 0.2%. The average percentage difference  $\Delta\sigma_{0.2AEP}$  between the calculated  $\sigma_y$  and  $\sigma_{0.2}$  as well as the average percentage difference  $\Delta\sigma_{pAEP}$  between the calculated  $\sigma_y$  and  $\sigma_p$  (from Table 4) are calculated and shown in Table 5. The large differences between the  $\sigma_y$  and  $\sigma_{0.2}$  indicate the irrationality of using  $\sigma_{0.2}$  as yield strength for DP and HSLA steels, while the small difference between  $\sigma_y$  and  $\sigma_p$  shows the potential of using  $\sigma_p$  as the yield strength for AHSS. An example of EPP and AEP models determined from an experimental  $\sigma$ - $\varepsilon$  curve (DP-700D01) is shown in Fig. 21.

In addition, the percentage difference of energy dissipation  $\Delta S_{EPP}$  between the experimental  $\sigma$ - $\varepsilon$  curve and the EPP model when adopting  $\sigma_y = \sigma_p$  is calculated and the averages are shown in Table 5. It is found that the energy dissipation of the EPP model is smaller than the actual experiment for all steels, and ranges from -1.0% to -13.3%. Similarly, the percentage difference of energy dissipation  $\Delta S_{AEP}$  between the experiments and the AEP model when adopting  $\sigma_y = \sigma_p$  is calculated and the averages are shown in Table 5. The average difference for each steel is less than 2%, which supports using  $\sigma_p$  as the yield strength in the AEP model. As expected, the AEP model gives a better fit to the data than the EPP model, but both models illustrate the necessity for using the recommended offset as given in Table 4 to represent the yield strength in conventional material models.

#### 7. Conclusion

Advanced high strength steels have different material properties compared with conventional steels. A series of tensile coupon tests on DP, HSLA, and MS steels with nominal yield strength from 340 MPa to 1200 MPa were carried out. Essential material properties including elastic modulus, 0.2% proof stress, ultimate strength and fracture elongation were determined. Coupons were cut from different directions along the sheet rolling direction and no obvious differences on material properties due to cutting directions was observed. Existing stress-strain models for conventional CFS and for stainless steels were discussed but they were not found to provide accurate fit with the AHSS database, especially around the yield region. An updated two-stage plus linear stress-strain model was therefore developed based on the Ramberg-Osgood model. Excellent fit was achieved between the proposed model and the AHSS database. For the required parameters of the proposed

model, a series of predictive equations were proposed to model the general stress-strain relationships of AHSS. A discussion on determination of yield strength was carried out by comparing the energy dissipation between experimental stress-strain curves and conventional stress-strain models, including the EPP model and the AEP model. The calculated yield strength of the conventional models showed poor fit with conventional 0.2% proof stress for DP and HSLA steels, but excellent consistency when the yield strength was represented by a novel recommended proof stress in the proposed stress-strain model. The stress-strain model and predictive equations presented herein could be utilized to model the constitutive relationship of AHSS in future work including analytical simulations.

## Data availability statement

The data that supports the findings of this study are available from the corresponding author upon reasonable request.

#### **Funding statement**

The first author was supported by the Wisconsin Alumni Research Foundation through an OVCRGEAward MSN237434.

## **Declaration of competing interest**

The authors declare that they have no known competing financial interests or personal relationships that could have appeared to influence the work reported in this paper.

## Acknowledgements

The authors would like to thank US Steel for donating the test material. Any opinions, findings, and conclusions or recommendations expressed in this material are those of the authors and do not necessarily reflect the views of the sponsors or other participants.

# References

- W. Yu, R.A. LaBoube, H. Chen, Cold-Formed Steel Design, 5th ed. John Wiley & Sons, Inc, 2019.
- [2] S. Keeler, M. Kimchi, P. Mooney, Advanced High-Strength Steels Application Guidelines, 6.0 ed. WorldAutoSteel, Brussels, Belgium, 2017.
- [3] R. Kuziak, R. Kawalla, S. Waengler, Advanced high strength steels for automotive industry, Arch. Civ. Mech. Eng. 8 (2008) 103–117.
- [4] ASTM, E8, Standard Test Methods for Tension Testing of Metallic Materials, 2016.
- [5] Y. Huang, B. Young, The art of coupon tests, J. Constr. Steel Res. 96 (2014) 159-175.
- [6] W. Ramberg, W.R. Osgood, Description of stress-strain curves by three parameters, National Advisory Committee For Aeronautics, 1943, Technical Note No. 902.
- [7] H.N. Hill, Determination of stress-strain relations from the offset yield strength values, Technical Note No. 927, Technical Report No. 927, National Advisory Committee for Aeronautics, Washington, D.C., USA, 1944.
- [8] E. Mirambell, E. Real, On the calculation of deflections in structural stainless steel beams: an experimental and numerical investigation, J. Constr. Steel Res. 54 (2000) 109–133.
- [9] K.J. Rasmussen, Full-range stress-strain curves for stainless steel alloys, J. Constr. Steel Res. 59 (2003) 47–61.
- [10] L. Gardner, D.A. Nethercot, Experiments on stainless steel hollow sections-part 1: material and cross-sectional behaviour, J. Constr. Steel Res. 60 (2004) 1291–1318.
- [11] H.-T. Li, B. Young, Cold-formed high strength steel shs and rhs beams at elevated temperatures, J. Constr. Steel Res. 158 (2019) 475–485.
- [12] P. Hradil, A. Talja, E. Real, E. Mirambell, B. Rossi, Generalized multistage mechanical model for nonlinear metallic materials, Thin-Walled Struct. 63 (2013) 63–69.
- [13] W.M. Quach, J.G. Teng, K.F. Chung, Three-stage full-range stress-strain model for stainless steels, J. Struct. Eng. 134 (2008) 1518–1527.
- [14] A. Olsson, Stainless Steel Plasticity: Material Modelling and Structural Applications, Ph.D. thesis Luleå tekniska universitet, 2001.
- [15] L. Gardner, M. Ashraf, Structural design for non-linear metallic materials, Eng. Struct. 28 (2006) 926–934.
- [16] W.M. Quach, Residual Stresses in Cold-Formed Steel Sections and their Effect on Column Behaviour, Ph.D. thesis Hong Kong Polytechnic University, 2005.
- [17] M. MacDonald, J. Rhodes, G. Taylor, Mechanical properties of stainless steel lipped channels, Int. Special. Conf. Cold-Form. Steel Struct. (2000).

- [18] K. Abdella, Inversion of a full-range stress-strain relation for stainless steel alloys, Int. J. Non-Linear Mech. 41 (2006) 456–463.
- [19] J.L. Ma, T.M. Chan, B. Young, Material properties and residual stresses of cold-formed high strength steel hollow sections, J. Constr. Steel Res. 109 (2015) 152–165.
- [20] L. Gardner, X. Yun, Description of stress-strain curves for cold-formed steels, Constr. Build. Mater. 189 (2018) 527–538.
- [21] Y. Huang, B. Young, Material properties of cold-formed lean duplex stainless steel sections, Thin-Walled Struct. 54 (2012) 72–81.
- [22] A.J. Sadowski, J.M. Rotter, T. Reinke, T. Ummenhofer, Statistical analysis of the material properties of selected structural carbon steels, Struct. Saf. 53 (2015) 26–35.
- [23] C. Ding, Z. Li, H. Blum, Y. Xia, B.W. Schafer, Ductility demands on CFS structural connections of advanced high strength steel, Proceedings of the Cold-Formed Steel Research Consortium Colloquium, 2020, URL: http://jhir.library.jhu.edu/handle/1774.2/63168
- [24] H.B. Blum, K.J. Rasmussen, Experimental investigation of long-span cold-formed steel double channel portal frames, J. Constr. Steel Res. 155 (2019) 316–330.
- [25] AISI, S100–16, North American Specification for the Design of Cold-Formed Steel Structural Members, AISI, Washington, DC, U.S.A., 2016
- [26] Y. Fukumoto, New constructional steels and structural stability, Eng. Struct. 18 (1996) 786–791.
- [27] P. Langenberg, Relation between design safety and y/t ratio in application of welded high strength structural steels, Proceedings of International Symposium on Applications of High Strength Steels in Modern Constructions and Bridge-Relationship of Design specifications, Safety and Y/T ratio. Beijing 2008, pp. 28–46.
- [28] W.M. Quach, J.F. Huang, Stress-strain models for light gauge steels, Proc. Eng. 14 (2011) 288–296.
- [29] C. Salmon, J. Johnson, F. Malhas, Steel Structures: Design and Behavior, 5 ed. Pearson, 2009.
- [30] C.A. Rogers, G.J. Hancock, Ductility of G550 Sheet Steels in Tension Elongation Measurements and Perforated Tests, Technical Report, The University of Sydney, Sydney, December 1996 1996.
- [31] N. Abdel-Rahman, K. Sivakumaran, Material properties models for analysis of cold-formed steel members, J. Struct. Eng. 123 (1997) 1135–1143.

# Glossary

E: elastic modulus

 $E_p$ : tangent modulus at p proof stress

 $E_{0.2}$ : tangent modulus at 0.2% proof stress;  $E_p$  when p = 0.002

σ: total stress

 $\sigma_{i}$ : stress of fracture point

 $\sigma_p$ : proof stress with a plastic strain of p defined by the offset of elastic modulus; stress of p offset point

 $\sigma_u$ : ultimate tensile strength

 $\sigma_{\rm v}$ : yield strength

 $\sigma_{0.2}$ : 0.2% proof stress;  $\sigma_p$  when p = 0.002

 $\sigma_{eu}$ : stress of the equivalent ultimate point

 $\varepsilon$ : total strain

 $\varepsilon_{f}$ : total strain of fracture point

 $\varepsilon_p$ : total strain corresponds to  $\sigma_p$ ; total strain of p offset point

 $\hat{\epsilon_u}$ : ultimate strain; total strain corresponds to  $\hat{\sigma_u}$ 

 $\varepsilon_y$ : total yield strain; total strain corresponds to  $\sigma_y$ 

 $\varepsilon_{0.2}$ : total strain corresponds to  $\sigma_{0.2}$ ;  $\varepsilon_p$  when p=0.002

 $\varepsilon_{eu}$ : strain of the equivalent ultimate point; total strain corresponds to  $\sigma_{eu}$ 

 $m\!:\!$  strain-hardening exponent of the second stage model (for two-stage or multi-stage Ramberg-Osgood model)

n: strain-hardening exponent of the whole model (for one-stage Ramberg-Osgood model) or of the first stage model (for two-stage or multi-stage Ramberg-Osgood model) p: offset of elastic modulus to define the proof stress

#### Acronyms

AEP model: artificial elastic plastic model with nonlinear strain hardening and softening AHSS: advanced high strength steels

DP steels: dual phase steel

EPP model: elastic perfect plastic model

HSLA steels: high-strength low-alloy steel

MS steels: martensitic steel